Carbon Nanotube Dispersion in Nematic Liquid Crystals: An Overview

Article *in* Progress in Materials Science · February 2016

DOI: 10.1016/j.pmatsci.2015.12.002

2 authors, including:

Satya Yadav
Banaras Hindu University
24 PUBLICATIONS **334** CITATIONS

SEE PROFILE

Progress in Materials Science 80 (2016) 38–76

Contents lists available at ScienceDirect

Progress in Materials Science

journal homepage: www.elsevier.com/locate/pmatsci

Carbon nanotube dispersion in nematic liquid crystals: An overview

Satya Prakash Yadav, Shri Singh *

Department of Physics, Banaras Hindu University, Varanasi 221005, India

ARTICLE INFO

Article history:
Received 15 April 2015
Received in revised form 5 December 2015
Accepted 23 December 2015
Available online 19 February 2016

Keywords:
Liquid crystal
Carbon nanotube
Dispersion of carbon nanotubes in liquid crystal

ABSTRACT

The aim of present review article is to present a comprehensive and current overview of scientific advancement in liquid crystal and carbon nanotube suspension. Particular attention has been paid to the recent developments and fundamental understanding of carbon nanotube dispersion in nematic liquid crystals. The dispersion and interaction of carbon nanotube in liquid crystal matrices and more elaborately the effect of dispersion on the properties of liquid crystalline materials has been extensively discussed. Recent progress has shown that even a very minute concentration of carbon nanotube in liquid crystals can have a reflective impact on the electrical and optical properties of liquid crystals. Liquid crystals provide a distinctive environment for controlling the alignment of carbon nanotubes whereas carbon nanotubes are important for the enhancement and fine-tuning of liquid crystalline properties. Potential applications of liquid crystal and carbon nanotube suspension are briefly discussed. Conclusion and future perspectives of this rapidly emerging field is provided at the end.

Contents

* Corresponding author. Tel.: +91 9935025416.
E-mail address: srisingh23@gmail.com (S. Singh).

http://dx.doi.org/10.1016/j.pmatsci.2015.12.002
0079-6425/

1. Introduction

A key issue or challenge about the applicability of carbon nanotubes (CNTs) is their propensity to form aggregates [1–5]. Most of the production methods for CNTs result in bundles of tubes or randomly oriented tubes. The random orientation and the entanglement of these tubes thus average out their anisotropic properties. Since most of the properties mechanical, electrical or optical are prominent along the tube length, the applications of CNTs in sensors, solar cells, field emission devices, probing devices, ultra-capacitors, electro and mechanical devices, etc. [6–11] are often more useful when they are uniformly aligned and disentangled. Several methods have been devised to align these CNTs – alignment during synthesis (using metal catalyst) and post synthesis techniques (application of electric and magnetic field, etc.). But all of these methods suffer with their own limitations and a high degree of orientation has not yet been achieved. One of the alternative ways to align these nanotubes is to impose the self organizing characteristic of liquid crystals (LCs) to CNTs. Even though the aspect ratio of CNTs is much higher than the LCs, at low concentration of CNTs in LCs, the mesogenic molecules are capable to slot in these tubes into its own orientation. The recent works clearly figure out how effective the LCs are in aligning these nanotubes, both thermotropic and lyotropic LCs [12–17]. Also the surface orientation of CNTs can be decorated by outlining the orientation of LC molecules either parallel to the surface (Homogenous Alignment) or perpendicular to the surface (Homeotropic Alignment) or twist alignment. The director reorientation of LCs can be superimposed to CNTs in LC/CNT suspension by elastic interaction with the application of electric or magnetic field of sufficient strength. Therefore, LC provides an environment for controlling the alignment of CNTs.

The improved optical contrast, observed by Heilmeier and Zanoni [18] in 1968 laid the foundation for the enhancement of properties of liquid crystalline materials by the dispersion of guest entities. This method has been established as a much easier way to perk up the properties of liquid crystals than to synthesize a new liquid crystalline material. In the last few decades the dispersants include polymers [19,20], nanoparticles [21,22], ferroelectric nanoparticles [23,24], quantum dots [25,26] and nanotubes [27,28] along with dyes [29–31]. In all the classes, CNT dispersed LC represents a very versatile system for the stepping up of mechanical, electrical and electro-optical properties of LCs and also the orientation of LC molecules on CNT surface. The shape anisotropy of the molecules of LC and CNTs make them a compatible companion. The configurational likeness of CNTs and LCs (both having rod like structure) escorts LCs to integrate CNTs into its own configuration effortlessly. This leads to potentially applicable and an interesting anisotropic composite system with improved physical properties, having low operating voltage and faster electro-optical response than pristine LC. Even small concentration of nanotubes in LC has shown to lead to large nonlinear optical effect [32,33]. Enhancement of electro-optical effects [34,35] as well as enhancement of dielectric and electrical properties [36,37] has also been reported, in recent years. Some new physical effects such as memory [38],

super-elongation of CNTs [39] and electro-hydrodynamics (EHDs) [38,40] have also been observed for these composite systems. It can be concluded that CNTs are cooperative in enhancing the properties of LCs.

A number of research papers [41–45] have appeared in recent years which reflect the technical importance of these composite systems. This anisotropic system has now become a very cost effective and simple method to align the CNTs and also for tailoring the properties of LCs, which is important for most of the possible technological applications. The subject has been reviewed by many others [46–51], but the effect of CNTs on the properties of LC has not been delineated. In this work, an attempt has been made to discuss all the effects and present a comprehensive and current overview of it. The outline of the present manuscript is as follows. The importance of CNTs and LCs for each other has already been discussed in previous paragraphs. In order to make article self contained, a brief introduction about LCs is given in Section 2. Section 3 deals with a concise introduction to the CNTs and their properties. Alignment and solubility problem with CNTs and their solution is discussed in Section 4. Homogeneous dispersion of CNTs in LCs is difficult. Therefore, three different methods adopted by the liquid crystal community, for properly dissolving these nanotubes are discussed in Section 5. Interaction of nanotubes with nematic molecules is addressed in Section 6. In Section 7, the orientation of CNTs within a LC matrix has been explored. Effects of orientation of CNTs on the properties of LCs are given in Section 8. In this section, the effects of CNTs on the properties of NLCs in terms of phase transition behavior, optical transmittance, memory effects, hysteresis, electrical conductivity and dielectric relaxation behavior, switching mechanism and rotational viscosity, ionic effect, voltage holding ration (VHR) and diffraction efficiency have been described extensively. The application of electric field leads to the orientation of the LC molecules and CNTs simultaneously in the suspension. The effect of electric field is delineated in Section 9, adjoining some new phenomenon such as super-elongation and translation motion of CNTs. Section 10 deals with the possible applications of these composite systems. The article ends in Section 11 with the conclusion and a brief comment on the future perspectives and challenges.

2. Liquid crystals: a brief introduction

From our basic perception, the order or the arrangement of the molecules in a crystal is usually represented by both positional and orientational order parameters. The molecules in crystalline solids are constrained both to occupy specific sites in lattice and orient their molecular axis in specific direction. On the other hand, in liquids the random diffusion of the molecules throughout the sample container and the tumbling of the molecular axis lead to the absence of both positional and orientational order. The mutual interaction of molecules in solids is much stronger as compared to the liquids. Liquid crystals (LCs) [52–58] are state of matter sharing symmetry and properties that are usually associated with both solids and liquids. The molecules in all liquid crystal phases (mesophases) diffuse about much like the molecules of liquid, but they do so maintaining some degree of orientational order and sometimes some positional order also [54,55]. The amount of order in the liquid crystal is quite small relative to crystal. There is a slight tendency of the molecules to point more in one direction than in others and to spend more time in some positions than in others. The arrangement of molecules in crystalline solid, liquid crystal and liquid phase is shown in Fig. 1.

It is well established that not all molecular shapes are able to form mesomorphic phases. The molecules must be elongated in shape or should be anisotropic in nature. The molecule must have some rigidity in its central region. The rigidity in the central region provides the stability to the mesophase. The flat segment of the molecules prefers the formation of liquid crystalline phase. The flexible group attached to the central region is responsible to the flowing or viscous nature of the liquid crystalline phase.

Based on the method of formation, liquid crystals can be categorized in (i) Lyotropic Liquid Crystal and (ii) Thermotropic Liquid Crystal. In thermotropic liquid crystals, mesomorphic behavior is defined by the temperature. Lyotropic phases are formed in solution. This phase is formed when an amphiphilic molecule (having both hydrophilic and hydrophobic groups) is dissolved in solvent. The concentration of amphiphilic molecules and the nature of solvent decide the phase behavior [52]. On the basis of

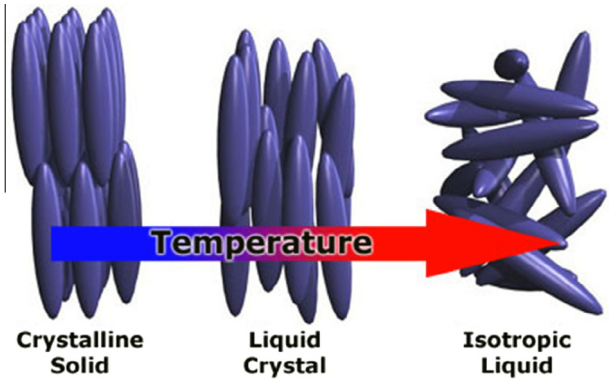

Fig. 1. Basic structural difference among crystalline solid, liquid crystal and isotropic liquid.

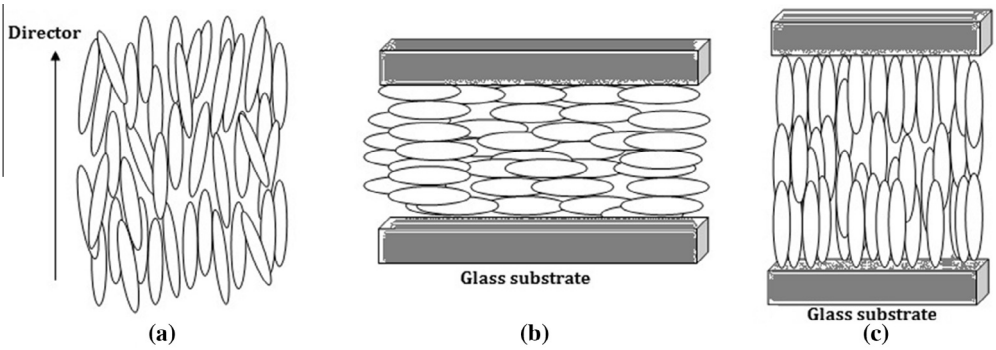

Fig. 2. (a) Orientation and arrangement of molecules in nematic liquid crystal and (b) homogenous and (c) homeotropic alignment of molecules on glass surface.

the shape of the molecules three types of LCs are designated – Calamitic (rod shape), disk shape and bend core shape. These classifications can further be subdivided into nematic and smectic phases. This subdivision is based on the molecular arrangement. Nematic phase is governed by a long range orientational order. In this phase, the center of gravity of molecules distribute randomly. There is no long range correlation between the centers of the mass of the molecules. In other words; the center of mass of the molecules has three dimensional translational freedoms [52]. A short range positional order exists, similar to liquid phase. The molecules on the average are aligned with their long molecular axis parallel to each other. This preferred direction is termed as director. The direction of the optic axis in nematic liquid crystal is in the direction of director. There exists rotational symmetry around director. The nematic phase is cylindrically symmetric with respect to director and it possesses a mirror plane perpendicular to the director [57]. The constituent molecule rotates (freely or hindered) around their long and short axis. The viscosities of the nematic phase are of the same order of magnitude as that of liquid phase. The unaligned nematic liquid crystals (NLCs) are similar to a polycrystalline power, where every domain has different orientation of the molecules. Uniform orientation of the molecules throughout the sample in a preferred direction can be achieved by a suitable surface treatment. The molecules can be aligned either parallel to the surface (homogenous or planar alignment) or perpendicular to the surface (homeotropic alignment). Two surface treatments can be used to create twist distortion to the nematic sample. A simplified picture of the relative orientation of the molecules in nematic phase is shown in Fig. 2.

Smectic phases are characterized by orientational as well as positional order at least in one dimension. On the average, the centers of the molecules are arranged in equidistant planes. Smectic phases are subdivided into SmA, SmB, SmC, etc. These phases differ in their orientation of the preferred direction of the molecules with respect to the layer normal and the organization of the center of the molecules within the layer (52–58, for more details).

The amount of order in liquid crystals is defined by parameter S, known as orientational order parameter. The parameter S is the second term in the expansion of the cylindrical distribution function of molecules in Legendre polynomial series [57]. Mathematically, it is given as $S = \langle 3\mathrm{Cos}^2\theta - 1\rangle/2$, where θ is the angle between the axis of an individual molecules and the director of the liquid crystal. For a prefect crystal $S = 1$ and $S = 0$ for liquids. S generally lies between 0.2 and 0.9 for liquid crystals.

3. Carbon nanotubes: a brief introduction

CNTs belong to the fullerene family and are cylindrical in shape with very high aspect ratio >1000. Length of the CNTs can be of the order of millimeters; however, the diameter of the tube ranges in few nanometers [59–63]. These tubes can be visualized as thick layer of graphene sheet rolled in the form of hollow cylinder. These tubes were first exposed by Iijima in 1991 [64] during the production of fullerene (C_{60}) using arc discharge method. The nanotubes produced were multiwall carbon nanotubes (MWCNTs). Latter in 1993, Iijima and Ichihashi [65] successfully manufactured single wall carbon nanotubes (SWCNTs) by means of metal catalyst in arc discharge method. Since then these anisotropic nanotubes have got much consideration because of their unique electrical, thermal and mechanical properties [50,66–68]. The nature of bonding in CNTs is sp^2 type, same as in graphene. Naturally CNTs occur in two forms: SWCNTs and MWCNTs. The SWCNTs can be conceptualized as a thick layer of graphene sheet turned around in the form of cylinder same as the rolling of newspaper. The typical diameter ranges in 1–2 nm and length in several microns and some time in mm. MWCNTs can be visualized as concentric cylinders, where several tubes are nested inside each other. The typical diameter for these nanotubes lies in the range of 5–50 nm and length in several microns. MWCNTs structure can be portrayed in two different models. In Russian Doll Model, nanotubes are visualized as arranged in concentric cylinder, one casing another. In Parchment Model, a single graphene sheet is rolled in such a manner that nested cylindrical tubes appear. The spacing between two adjacent nanotubes is approximately 3–4 A^0.

The way graphene sheet can be rolled is represented by two indices n and m. The number n and m denote the number of unit vectors along two directions in the crystal lattice of graphene: one along the zigzag bonds called zigzag line and another along the hexagonal known as armchair line [69]. Both lines are shown in Fig. 3. The circumference is denoted by $C = n\hat{a}_1 + m\hat{a}_2$. If $m = 0$ the vectors C coincides with zigzag line and now if graphene sheet is rolled along this line, zigzag nanotubes is obtained. For $n = m$ the vector C coincides with the armchair line and the rolling along this line produces armchair nanotubes. For $n > m$ and $m \neq 0$ the produced nanotubes are chiral nanotubes. The selection of rolling axis about the hexagonal structure of graphene changes the electrical properties of nanotubes from insulation to conducting and vice versa. Typical carbon nanotube structures are shown in Fig. 3.

The SWCNT and MWCNT are usually produced by arc discharge, laser ablation, chemical vapor deposition (CVD), super growth CVD, gas phase catalytic process or high pressure carbon monoxide (HiPCo) methods [70–76]. In arc discharge method, a current of about 50 A is applied across two graphite electrodes in a helium atmosphere. This results into graphite evaporation. Some part of evaporation gets collected on the vessel wall and some on the cathode. The carbon collected at cathode is nanotubes. The SWCNTs are produced by this method using some metals as catalyst or mixture of metals (Fe, Co, Ni, Ni–Co, Co–Y, Ni–Y, etc.). In laser ablation process, intense laser pulse is used to vaporize the graphite in high temperature reactor and in the presence of inter gas. The vaporized carbon finally got condensed in the form of nanotubes at the cooler wall of the reactor. The application of high temperature in these two processes results in the high crystallinity of the nanotubes. However, unfortunately, a considerable quantity of unwanted particles or impurities such as amorphous carbon, graphite polyhedrons, metal nanoparticles, and fullerene is also produced. In CVD method CNTs are grown on metal catalyst substrate. To achieve higher yield, it is necessary to increase the surface area

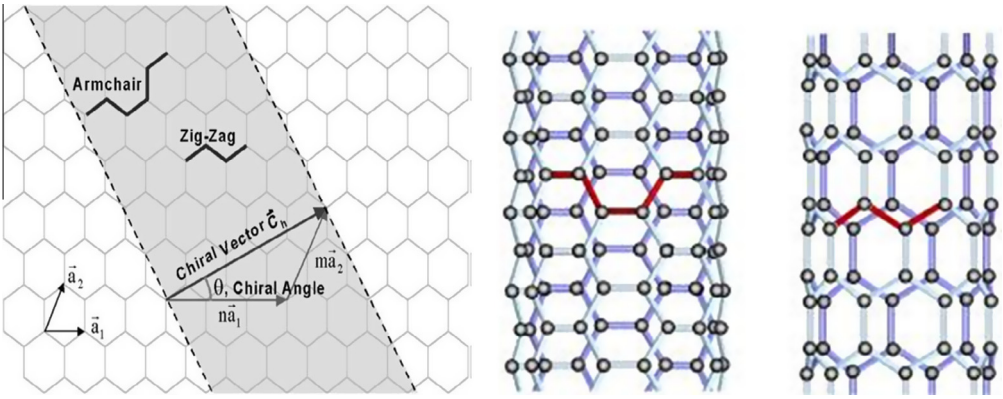

Fig. 3. Typical carbon nanotube structures.

Table 1
Comparison of different production methods.

Process/property	Arc discharge	Laser ablation	CVD
Raw material availability	Difficult	Difficult	Easy, abundantly available
Energy requirement	High	High	Moderate
Process control	Difficult	Difficult	Easy, can be automated
Reactor design	Difficult	Difficult	Designed as large scale process
Production rate	Low	Low	High
Purity of product	High	High	High
Yield of process	Moderate (70%)	High (80–85%)	High (95–99%)
Post treatment requirement	Required refining	Require refining	No extensive refining required
Process nature type (Continuous or Batch type)	Batch type	Batch type	Continuous
Per unit cost	High	High	Low

of the catalyst. For the purpose metal nanoparticles such as Al_2O_3 and MgO are used in support to catalyst. The substrate is heated up to 700 °C. The size of CNTs depends on the diameter of nanoparticles. In super growth CVD process the activity and the life time of the catalyst are enhanced by the addition of water into the CVD reactor. HiPCo method uses $Fe(Co)_5$ as a catalyst and CO acts as feedstock. In an another method (CoMoCat method) Co and Mo is used as a catalyst and continuous flow of CO gas at pressure of 1–10 atm and temperature 700–950 °C is maintained. A comparison of different production method is shown in Table 1 [77].

Also when these tubes are synthesized they exit in a mix of different nanotubes containing metallic and semiconducting nanotubes. These tubes can be separated by using high voltage, leading to flow of heavy current through the metallic tubes, causing them to vaporize and leaving behind only semiconducting tubes [78,79].

The high Young's modulus and tensile strength of the nanotubes makes them mechanically rigid and stronger as compared to diamond and steel. This high mechanical strength is due to the covalent bond (sp^2) among the individual carbon atoms. CNTs have Young's modulus over 1000 GPa, almost 5–6 times superior to high strength steel (200 GPa) and comparable to diamond [80–83]. The tensile strength of these CNTs lays in the range 11–65 GPa. The density of CNTs are much lower i.e. 1.33–1.4 g/cm^3, which is almost 1/6 of the weight of steel. The rolling of the graphene sheet decides the metallic or semiconducting nature of the tube. All armchair nanotubes are metallic in nature and zig-zag and chiral tubes are semiconducting. The electronic transport in CNTs is along the long tube axis and occurs ballistically. The CNTs are equipped to handle a current density of about 10^9–10^{10} A/cm^2 without being heated too much and also resistivity of the tubes remains almost unaffected up to 250 °C [84,85]. Heat transmission competence of CNTs are also very good i.e. 6000 W/m K,

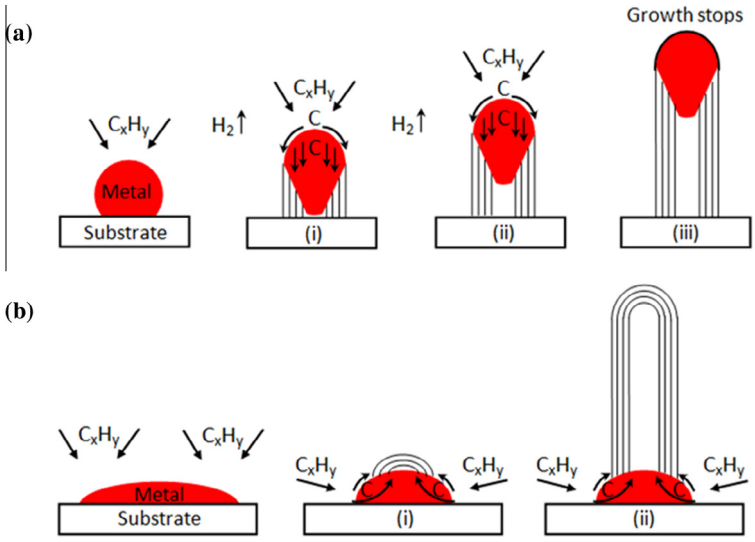

Fig. 4. Two growth mechanisms for the production of CNTs [100].

almost two times to that of diamond (3000 W/m K). CNTs are thermally steady up to very high temperature, in vacuum they can withstand up to 2500 °C and in air up to 750 °C [86–88].

4. Alignment and dispersion of carbon nanotubes

Most of the properties of CNTs that are technically important such as mechanical, electrical or optical are prominent along the tube length. Therefore, proper alignment of these tubes is important. However, whatever the production methods are known, they produce entangled tubes or randomly orientated tubes. Some attempts have been made to align these nanotubes in preferred direction [89–98]. The methods can be basically classified in two categories: during growth and post synthesis techniques [[99] and references therein].

In general two growth mechanisms are used during the production of CNTs [100]: (a) tip growth and (b) base growth mechanism. These growth mechanisms are common to all the production methods. In both the mechanism three steps are followed. At first, metal catalyst is settled down on a support surface and a round or a pear shaped precursor is formed on the catalyst surface. Secondly, the carbon diffuses on the sides of the precursor. In base growth mechanism, the carbon nanotubes grow vertically from the metal catalyst surface. In this process metal catalyst remains attached to the surface. In tip growth process, the metal catalyst disengages from the support surface and remains attached to the tip of the growing nanotubes. Varying the size of metal catalyst, SWCNT or MWCNT can be grown. The illustration of the process is shown in Fig. 4 [100].

To achieve the aligned nanotubes during growth, nanoparticles of metal catalyst such as Co, Ni, Mo, and Fe are used. Nanotubes are grown on this highly concentrated catalyst [100–102]. The high concentration of catalyst prevents the nanotubes to bend down. The use of these metal nanoparticles has their own drawbacks. The attached nanoparticles to CNTs change the intrinsic properties of CNTs to some level. These nanoparticles can be removed by the use of strong acids [103,104]. Application of electric field during the growth, normal to the substrate, helps the tube to align more preferably in one direction. Direction and strength of electric field allows controlling the alignment and the structure of CNTs. Low density of catalyst can be used to align the CNTs along the substrate on oriented sapphire or trenched silicon [105,106]. Electron beam induced deposition, can also produce aligned tubes. Aligned nanotubes have also been realized by the surface modification of substrate [12]. Growth of nanotubes inside the nano-channels of various templates such as mesoporous silica,

alumina, aluminophosphate or zeolite results in vertical alignment of the nanotubes [73,107–110]. The pore size of the nano-channels allows in controlling the diameter of CNTs.

The nanotubes can be aligned after their production also. This generally requires mixture of nanotubes and dispersants. The dispersants should be removed after the alignment is achieved. The produced nanotubes are first dispersed either in polymer or surfactant (usually known as dispersant) using ultrasonic and then using centrifugation the concentrated nanotubes are separated from well dispersed ones. In case of CNTs embedded in polymer, either thin film is stretched or application of uniaxial pressure of ~10 kbar aligns the nanotubes [111,112]. Rubbing the polymer film after softening, either wetting in or warming, can also align the nanotubes [113]. In case of hard polymers such as polystyrene or polyurethane, nanotubes can be aligned in fractured gap by overstretching the polymer [114,115]. Aligned CNTs have also been realized through the filtration of well dispersed nanotubes through porous membranes [116]. Application of electric or magnetic field will also result in well aligned tubes [117,118]. A tiny droplet of a well dispersed CNT suspension is deposited on a substrate having interdigitated electrode. Application of electric field aligns the nanotubes between the electrodes. In another method, solution containing well dispersed CNTs is deposited on the substrate and film is dried in the presence of magnetic field. The nanotubes align to the direction of magnetic field. Due to weak magnetism of CNTs, a high strength of magnetic field is required for the alignment. In case of electric field only ac field can be applied because dc field results in accumulation of CNTs on one electrode. The drawback of these techniques is that alignment obtained is not everlasting, it decays with time. Gas flow and Langmuir–Blodgett (LB) techniques are also effective [119,120]. In gas flow technique a well dispersed CNT solution is deposited onto the substrate and gas flow at a speed of 10 cm/s is applied. The flow simultaneously spreads the drop, dries them and aligns the nanotube along the flow direction. In LB technique substrate is slowly dipped into the solution of well dispersed NTs and then pulling out slowly. CNTs get aligned in the dipping direction. Thickness can be controlled by number of dips and pulling speed.

The efficient dispersion and the breaking of the CNT aggregates is a great challenge. When CNTs are dispersed in solvent in low concentration, the forces form the solvent molecules on CNTs are same in every direction and hence, no resulting force acts on the nanotube. However, when the concentration is raised beyond a certain limit, the space between two adjacent CNTs becomes inaccessible for the solvent molecules. This inaccessibility leads to the imbalanced forces and as a result CNTs come closer to each other. This decreased separation between the nanotubes further lead to the aggregation. This also prevents the high loading of CNTs to disperse into most of the known organic solvents [121,122]. The prerequisite for proper dispersion of CNTs in any solvent is that CNT–Solvent interaction must be stronger than the CNT–CNT and Solvent–Solvent interactions. Recently, it has been realized that dispersion of NTs in solvents require compounds composed of aromatic moiety and solvophilic moiety. Solvents having hydrophobic or hydrophilic moiety can disperse CNTs in water and alcohols and in non-polar solvents, respectively. The recent studies point out that organic solvents such as *N*-methylpyrrolidone (NMP), *N*,*N*-dimethylformamide (DMF), 1,2-dicholoroethane, Ethanol, Chloroform have potential to disperse these nanotubes [123–126]. In addition, Maeda et al. [127] have shown that tetrahydrofuran (THF)/octylamine solution also disperse NTs effectively. Nicholas et al. [116] has successfully demonstrated that chlorosulfonic acid acts as a good solvent for SWCNTs, DWCNTs (Double Wall CNTs) and MWCNTs. Instead of using organic solvents, use of surfactants is also preferred. Some commonly used surfactants are sodium dodecylsulfate (SDS), sodium dodecyl benzenesulfonate (SDBS), sodium cholate (SC) [17,128,129]. Some biological polyelectrolytes such as DNA and Hyaluronic acid (HA) have also been useful for CNT dispersion [130–132]. Solubility in organic or aqueous media can also be obtained by either covalent functionalization or non-covalent functionalization (Ionic) of NTs [133–136]. The Ionic functionalization of tubes is better than the covalent functionalization, as it doesn't transform the electronic properties of nanotubes. The protonation of CNTs sidewalls by super acids results in dispersion of high concentration of tubes in organic solvents. Therefore, proper selection of dispersing agent is important one as it can minimize the chemical modification or damage as compared to other dispersing agents.

5. Dispersion of carbon nanotubes in liquid crystals

The LC community generally follows three methods for dispersing nanotubes in LCs. In first approach, nanotubes are directly mixed with LCs followed by the percolation of mixture to remove the unwanted carbon particles such as graphite and amorphous carbon [32,33,137]. Then the mixture is sonicated for some time to properly disperse the nanotubes. In another approach, CNTs are first dispersed in proper solvent and then mixed with liquid crystal medium [138,139]. The prepared solution is then properly sonicated to scatter the agglomeration of CNTs. The solvent is evaporated thermally and the remaining mixer left only with LC and CNT. In third approach, before dispersing CNT in LC, CNTs are functionalized either by surface encapsulation or covalent functionalization [140,141]. All the three methods discussed above have their limitations. In first approach, good dispersion is limited to only 0.1 wt% nanotubes in LC. Also after percolation it is very hard to notify about the accurate concentration of nanotubes in LCs. In second approach, it is very hard to completely evaporate the solvent; some traces still remain in the suspension. In third approach, surface modification leads to the change in the intrinsic properties of CNTs.

It is always recommended to use the pretreated CNTs before dispersing in LCs. Usually ball milling procedure is employed. The adoption of this method shatters the CNT aggregates and also shortens the length. For long term stabilization, the prepared LC/CNT suspension should always be kept in mesophase, not in isotropic phase. Also, one should not go far away from the nematic to isotropic transition temperature (T_{NI}) during the sample cell filling.[1] Temperature plays a major role in the formation of aggregates of nanotubes in liquid crystals. The increased kinetic energy (due to increased temperature) of the nanotubes leads to the increased interaction and finally to the formation of aggregates. Also the adsorption of the liquid crystal molecules on the surface of CNT introduces a short range positional order and this minimizes the entropy of the suspension. The anisotropic viscosity of the liquid crystals also plays a decisive role to counteract the CNT aggregation. The reorientation of nanotubes is highly hindered in the direction perpendicular to the director. The inter-tube contacts are counteracted by the viscosities. Therefore, keeping the suspension in liquid crystal phase stabilizes the system.

The formation of aggregation is found to be similar for SWCNT and MWCNT [142]. It is also stated that stirring and sonication improves the dispersion quality of CNTs [143]. The dispersion process must be followed by centrifugation and decantation step, to remove the extra impurities and remaining large scale aggregation. The time for all the process should be optimized for every LC.

A step toward the solution of miscibility has been moved by Ji and workers [139], using liquid crystal polymer. A high concentration of CNTs (1 wt%) in LCs is accomplished which is stable for over 6 months. A suitable liquid crystalline polymeric surfactant is required for different LCs. Recently, CNTs functionalized with LC has been found to disperse in ethanol and miscible in LC medium [144]. The polarizing optical microscope reveals that high quantity of CNT (~5 wt%) is aligned without aggregation.

A new method of improving dispersion of CNTs in LC using ac electric field is proposed by Tie and workers [145]. The suspension without field shows average cluster size of ~1.3 μm and it is reduced to 0.6 μm after the application of electric field ~2.1 V/μm. Even after time duration of 48 h no aggregation is observed. It is stated that in the absence of electric field CNTs are extended into the form of bundles. With the application of electric field of sufficient strength, the CNTs outstretched which results in debundling. The exposed CNT surfaces now anchor LC molecules strongly, which prevents further re-aggregation of nanotubes and assuring the improved solubility. Another report claims that the process of EHD or turbulence flow results in the grinding of the aggregates of nanotubes and improves the dispersion of CNT in NLC matrix [146]. Song and Windle [147] demonstrated that solubility and stability of colloidal suspension of MWCNT in water can be enhanced by the acid treatment. The dispersion ability of CNT in LC is also improved by the use of Laponite. The Laponite plates surrounding (due to strong anchoring to CNT) the CNT, destroys the aggregation and disintegrates the CNT bundles [148].

[1] Parallel plate capacitor type sample holders are used to investigate the liquid crystalline properties. The liquid crystal is filled in these sample holders by capillary action. For the homogenous filling of liquid crystals in these sample holders, it is required that the filling process must be done in isotropic phase.

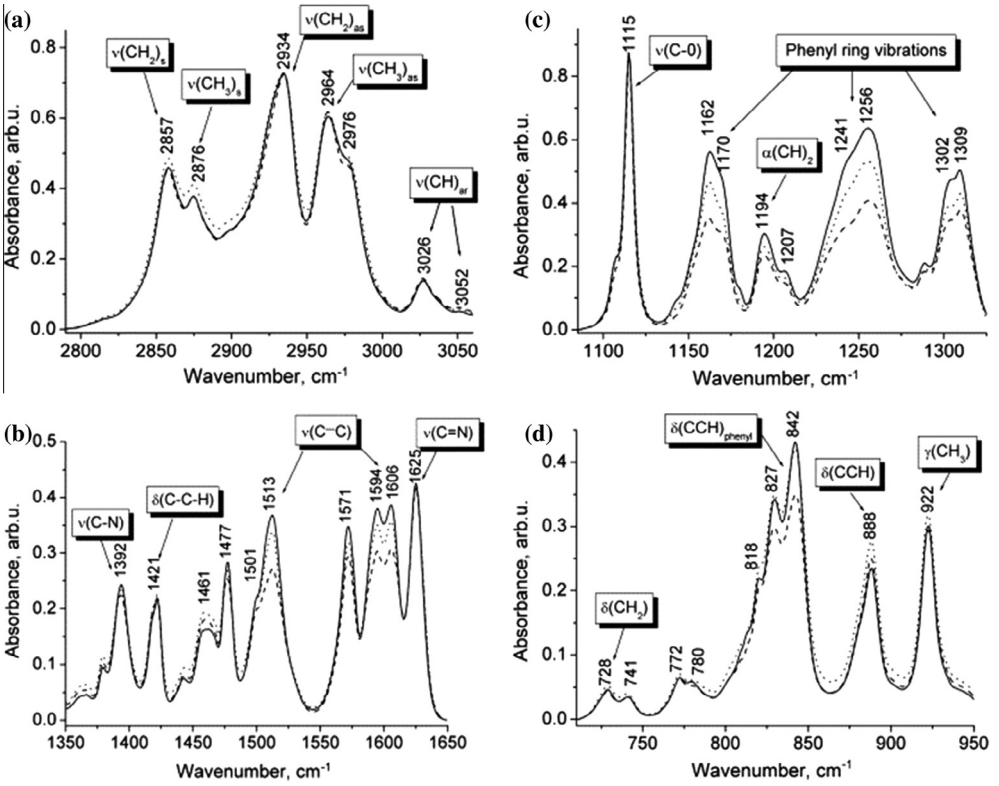

Fig. 5. Fragments of IR absorption spectra of pure EBBA (solid line) and MWCNTs/EBBA composites in the region of C—H stretching (a); ν(C—C) and ν(C—N) (b); and out of plane C—C—H bending, CH_3 twisting and central core C—C—CH bending (d); vibration for different MWCNT concentrations: 0.5 wt% (dashed) and 0.05 wt% (dotted line) [with permission Ref. [149]].

6. Interaction of carbon nanotubes with nematic molecules

Trushkevych and coworkers [140] reported a comparative study of the available tools to characterize the CNT dispersed LCs. The range, applicability and limitations of these tools are well studied. For a very minute concentration of CNTs in LC, AFM (Atomic Force Microscopy), ESEM (Environmental Scanning Electron Microscope), TEM (Transmission Electron Microscope), Nanoparticle tracking analysis, Dynamic light scattering method and Optical microscopy are found to be informative and suitable. For higher concentration of NTs in LC, FTIR (Fourier Transform Infrared) spectroscopy and Polarized Raman spectroscopy is found to be the best one to investigate the interaction of nanotubes in LCs.

The FTIR spectroscopic data indicates the strong interaction between the MWCNTs and NLC molecules [149]. Fig. 5 shows the different absorption peaks in different wave number region for MWCNT/EBBA (EBBA = *N*-(4-Ethoxybenzylidene)-4-butylaniline) composite. In the spectral region of 2800–3100 cm^{-1} (assigned to C—H stretching vibration) the presence of MWCNT does not amend the peak position or band width. The increase in bandwidth of CH_2 stretching band at lower concentration of NT results due to disordered butyl fragment in EBBA molecule. Also the vibration related with C═N, C—N, C—C—H stretching remains unaltered. However, intensity peak of absorption band related to phenyl ring stretching in the spectral region of 1350–1650 cm^{-1}, decreases with increasing concentration of MWCNTs in EBBA. This decrease in intensity indicates toward the π–π interaction between MWCNT and EBBA molecules. As the concentration of MWCNT is increased, the interaction between EBBA molecule and CNT surface increases. The interaction between phenyl rings of benzylidene aniline core

and surface of MWCNT results in π–π stacking. A more pronounced effect in the redistribution of intensity of absorption band of bending vibration of phenyl ring in the spectral region of 1250–1350 cm^{-1} has been observed. These vibrations are centered on 1309, 1302, 1256, 1241, 1170 and 1162 cm^{-1}. However, vibration related to C—C at 1194 cm^{-1} and C—O at 115 cm^{-1} remains untouched. In the spectral region of 600–950 cm^{-1} the out of plane phenyl C—C—H bending vibration at 842, 827, and 818 cm^{-1} decrease as the concentration of NTs is increased. This further confirms that interaction between MWCNT and EBBA molecule is solely governed by the core part of EBBA molecule.

The radial breathing mode (RBM) in Raman spectra, which is related with the vibration perpendicular to the tube axis, is very sensitive to the interaction of guest entity with tube surface [150]. Comparing the Raman spectra in RBM of CNT and 5CB + CNT (5CB = 4-Cyano-4′-pentylbiphenyl), four RBM peaks were detected which were shifted toward the right side. The observed shift was associated with the π–π stacking interaction around the aromatic core structure of 5CB and CNT surface. It is worth mentioning here that no such shift was observed with other LC having similar structure but no phenyl ring. The strength of interaction between MBBA (*N*-(4-Methoxybenzylidene)-4-butylaniline) and CNT is enhanced by the π–π stacking through the hexagonal rings in MBBA molecule and CNT wall [151].

A systematic investigation on the interaction between LC and CNT was performed by Park and group [152] using density functional approach. For the purpose they used tri-fluorophenyl2 (TFP2) LC. A systematic view of top and side edge of LC molecule anchored on the edge is shown in Fig. 6. The head group of LC interacted with the CNT wall, leading to a π–π stacking among the hexagonal rings of LC and CNT, with the closed separation of 3 A^0. On the other hand tail group was repelled by the CNT wall with large separation of 5 A^0. The calculated binding energy turns out to be −2 eV. The significant amount of charge transfer among LC and CNT, which is asymmetrical, leads to the permanent dipole moment in CNT. The charge transfer takes place from highest occupied molecular orbit (HOMO) localized at the head part of the LC molecules to CNT [153]. This dipole moment causes the translational motion of CNTs under the applied electric field, as observed by Baik et al. [154].

In summary, the interaction between CNT and LC molecules involve three main contributions: (1) the Vander Waals interaction, (2) overlap of the molecular orbits, and (3) charge transfer between CNT and LC molecules. The HOMO of LC molecules interacts with the LUMO of the CNT. A considerable amount of charge transfer takes place between the nanotubes and LC molecules. This leads to a permanent dipole moment in CNTs. Therefore, an additional electrostatic force exists between CNT and LC molecules. As a consequence, nematic molecules get aligned on the surface of CNTs. This leads to a certain amount of positional order in LC/CNT suspension.

7. Orientation of carbon nanotubes within the nematic matrix

Since past four decades, dispersion of guest particles in liquid crystalline medium has been an active area of research. Serious efforts have been made to study and explore the orientation of the particles in these systems. Early studies were concentrated around the distortion caused and the orientation of the rod like particle in NLC. Brochard and de Gennes [155] tried to explain the long range distortion induced in nematic matrix by dispersion of elongated particles (particle volume fraction of order of 10^{-3}). It was found that for an elongated magnetic grain of length L and diameter d ($L/d \approx 10$), the distortion is minimum when long axis of the grain coincides with the orientation of liquid crystal. However, an energy equivalent to KL, where K is the average frank elastic constant, is required to align these grains perpendicular to LC director. The extensive solution to this problem was further clarified by Burylov and Raikher [156,157]. It is mentioned that depending on the type and strength of the coupling anisotropic solid particles embedded in NLC can attain an equilibrium position either parallel or perpendicular to the nematic director. The orientation of any foreign particle is governed by a dimensionless parameter ω, where ω is the ratio of particles radius to the extrapolation length of the nematic. In Molecular dynamics and Monte Carlo simulations [158], it was demonstrated that for a particle of length greater than its transverse length, dispersed in NLC, the disclination lines of strength −1 evolves spontaneously into two −1/2 disclination lines. However, for a particle of transverse length, comparable to its length, −1/2 rings defect encircling the particle is stable. By changing the particle tilt angle with respect to nematic director, the orientation of this ring defect can be changed

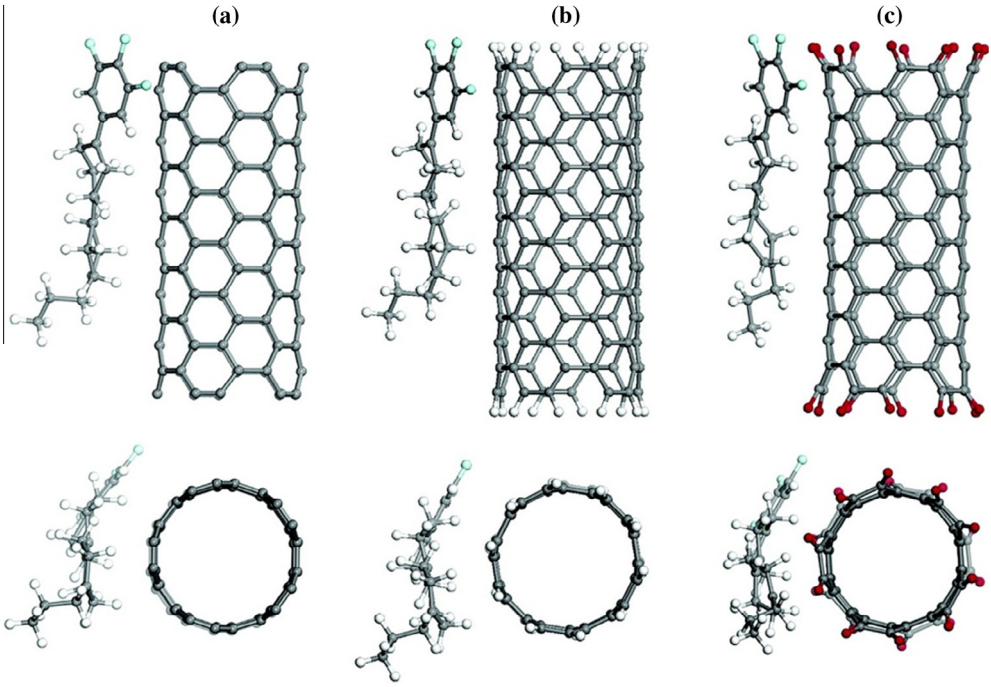

Fig. 6. Side and top views of the LC molecule anchored on the edge site of (a) the bare CNT, (b) the H-CNT, and (c) the O-CNT [with permission Ref. [152]].

as the torque experienced by particle depends on its orientation. It is also found that nematic phase is biaxial near the defect nuclei. For tilt angle $\theta = 0^\circ$ the orientation of the particle is not stable and some symmetry breaking is noticed. A stable state is obtained when orientation of the particle becomes perpendicular to the nematic director i.e. $\theta = 90^\circ$. The interaction between particle and wall is also considered. As the particle moves closer to the wall the torque increases and the orientation and equilibrium is affected. Considering the forced between the particle [159], defect lines are formed near the particle and are perpendicular to the director for large separation of particles. This director distortion vanishes very rapidly and the core (nuclei) region extends over few molecular lengths. As the separation between the particles decreases, the defect structure changes. The original defect structure (circular: when particles are well separated) loses their shape and finally when two particles are in close contact with each other, two out of four defects vanishes. The depletion force parallel to the particles separation play dominant role and is almost independent of the relative positions of the defect. The force per unit length show wavy nature which is due to the contribution of density modulation. The nonzero tangential component of the force (force perpendicular to the particles separation vector) decays with particle separation and try to align the separation vector perpendicular to the director for $\alpha = \pi/4$. A large variation for value of tangential component of force for $\alpha = 0$ and $\pi/2$ has been observed. This randomness is due to shifting of defects when particles move close to each other. An energy barrier of order of k_BT exists between two configurations for small particles. Therefore, defects can switch between these two configurations during the simulation run. This shifting of defects averages out the tangential component of force but does not affect the parallel component of force. Also the drifting process slows down the molecular simulation process and thus leads to large scattering in the value of tangential components.

Opposite to the results of Andrienko et al. [158,159], an axial symmetry is predicted for the orientation of particle along nematic director [160]. The discrepancies observed is attributed to the liquid crystal density inhomogeneity and packing around the elongated nanoparticles, which is not

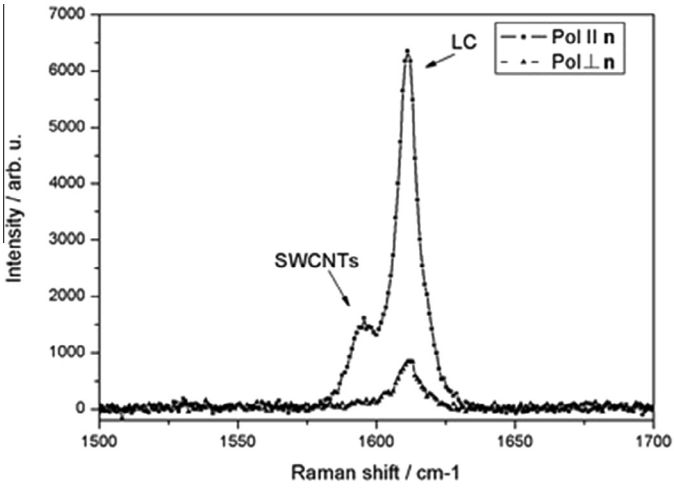

Fig. 7. The G band regime of Raman spectra from a HiPCo SWCNT-5CB LC composite taken with the polarization of the excitation laser parallel and perpendicular to the director. The large polarization dependence of the intensities of both peaks shows that the CNTs and LC are aligned equally [with permission Ref. [47]].

considered by Andrienko et al. The continuous symmetry breaking results in the formation of nematic domains, after quenching [161]. However, the presence of nanoparticles stabilizes the domain pattern.

Polarized Raman spectroscopy to detect the alignment of SWCNTs in LC matrix has also been used [162,163]. The unique structure of CNTs illustrates characteristic peaks in Raman spectra. The Radial Breathing Modes (RBMs) around 75–300 cm^{-1}, the D band between 1330 and 1360 cm^{-1} and the G band around 1580 cm^{-1} are observed. The RBMs originate as a result of vibrations perpendicular to the long axis of the CNT. The D band denotes the defects in CNT structure and the G band originates due to the tangential stretching oscillations. The intensity of the Raman signal is used to differentiate the preferred orientation of the nanotubes. The G band regime of Raman spectra for SWCNT/5CB composite is shown in Fig. 7. Highest intensity is observed when tubes are aligned along the director (or polarization is parallel to director) and lowest when they are perpendicular to the director (or polarization is perpendicular to the director). The observed mode intensity resulted to be higher for light parallel to the LC director than in the perpendicular direction, which indicates that the alignment of the SWCNTs is in the same direction as the LC director.

Earlier work by Adams and coworkers [164] successfully demonstrate that LC can be easily oriented on carbon fiber surface and also to micro sized glass roads [165]. Homeotropic alignment of LCs was also achieved on the substrate decorated with CNT [166]. Sparing CNT films on ITO coated glass plate introduces the uniform alignment of NLC on macroscopic level [167]. It is argued that unidirectional roughness of the substrate surface contributes to the planar alignment.

The structural ordering of MWCNT in LC host can also be tested by analyzing the transmittance vs. reduced temperature curve as observed by Lisetski et al. [168]. The nematic phase of NLC/CNT suspension suggests the parallel orientation of CNT in LC matrix. Also the change in transmittance with increasing concentration of MWCNT suggests that NT is well ordered in LC matrix. The orientation of SWCNT in a nematic suspension of colloidal rod like fd virus has also been studied where size of fd virus host particle was greater and thicker than the CNT. The orientational order of CNT is (0.1–0.35) found to be less than the host particle orientation order (0.55–0.75) [169]. An orientational order of $S = 0.9$ is determined for E7/MWCNT (E7 is a mixture of biphenyl and triphenyl) suspension which is greater than the orientational order of nematic LC itself [27]. The highly ordered arrangement of CNTs is attributed to the additional flow alignment during cell filling and low thermal fluctuation due to higher length and mass of CNTs.

When the concentration of NTs is increased in LC/CNT suspension, the interaction between the nanotubes becomes important to decide the behavior of system. At some critical concentration (percolation threshold) transition from non-conducting to conducting state occurs. A percolation threshold of $c = 0.1$ wt% MWCNTs in EBBA is noticed. However, individual aggregates appear even at some smaller concentration [170]. The fractal dimension d_f^3 for 3D aggregates is estimated to be 2.81, which is greater than the 3D random percolation value $d_f^3 = 2.5$. It predicts the ball like clusters (size of about 100 μm) having large cavity between them [170,171].

Kaya et al. [172] and Akkurt [173] observed a notable increase in order parameter in CNT dispersed in different dye doped nematic liquid crystals, owing to bridge formation among LC/LC and LC/dye conjugate systems by nanotubes. A maximum value of 0.77 has been attained when co-using red 60 dye and nanotube dopant in E63. Dolgov reports [146] the aggregation of CNTs which are clearly visible under polarizing microscope, single aggregates for $c < 0.02\%$ and in a form of continuous network when $c > 0.5\%$ in EBBA + CNT series. It was observed that very small concentration of CNTs in LC resulted in uniform distribution of tubes which almost remains invisible under polarizing microscope. The percolation threshold of $c = 0.025$–0.05 wt% was noticed for unmodified CNTs and was increased to $c = 0.1$–0.25 wt% for modified CNTs due to smaller aspect ratio [37]. In comparison to MLC6608 suspension, the density of CNT network is lower. The existence of aggregates of CNTs was extensively discussed by Minenko and group [174] using microscopy, differential scanning calorimetry, electrical conductivity, optical transmittance and singular optics. The formed *S* aggregates in 5CB + MWCNT suspension comprised of skeleton formed by the nanotubes and a shell of incorporated and adjacent nematic molecules. This can be visualized in the form of quasi-microscopic particle in the nematic matrix.

An interesting phenomenon of pseudonematic domains in the isotropic phase of CNT + LC suspension has been noticed by Basu et al. and others [42,150]. In the isotropic phase of 5CB with minute concentration of CNT (0.005 wt%), the average dielectric permittivity increases with the application of electric field and it doesn't relax back even when the field is turned off. The coupling between CNT and LC introduces pseudonematic domains in the isotropic media. These local domains reorient with applied field and result in increase of average dielectric permittivity. There is no restoring force in isotropic phase, therefore, domains remain oriented until they are heated or again reoriented with application of electric field.

The significant mechanical twist was observed in 5CB dispersed with a very small concentration of CNTs having chirality [138]. It was also noted that helical twist (in terms of P^{-1}) began to saturate in higher concentration region, $c \geqslant 0.0015$ and saturate at $c = 0.004$. It was believed that the aggregates of CNTs results in the saturation of P^{-1}.

The predefined orientation of CNTs is used to grow distinct local single crystals of SmC LC. The surface anchoring and surface memory effect of SWCNT/SiOx/ITO glass surface is found to be much stronger as compared to SiOx/ITO glass surface and bare ITO glass surface [175]. Lagerwall et al. and others [16,176] have successfully demonstrated that SWCNT can be easily dispersed and simultaneously can be aligned in lyotropic nematic liquid crystal of both disk and rod shaped micelles.

In another report, ferromagnetic NTs (CNT filled with α-Fe) in nematic liquid crystal (NLC) reveals that aggregates formed are elongated in shape and mostly oriented along the director [177]. The main contribution to the formation of these aggregates comes from the Vander Waals and magnetic interaction. Magnetic and orientation elastic interaction encourages the formation of elongated or anisotropic aggregates. Magnetic force also leads to orientation of magnetic CNTs along the director.

8. Effect of orientation of carbon nanotubes on various properties of nematic liquid crystals

8.1. Phase behavior

Considering the studies made earlier, Kralj and group [14,178–180] made an extensive and lucid study of phase behavior of the LC/CNT mixture. LC induced ordering of CNTs under weak and strong anchoring limits and CNT induced disorder of LCs are considered. The total free energy density per unit volume of LC/CNT mixture can be written as [14,174,178]

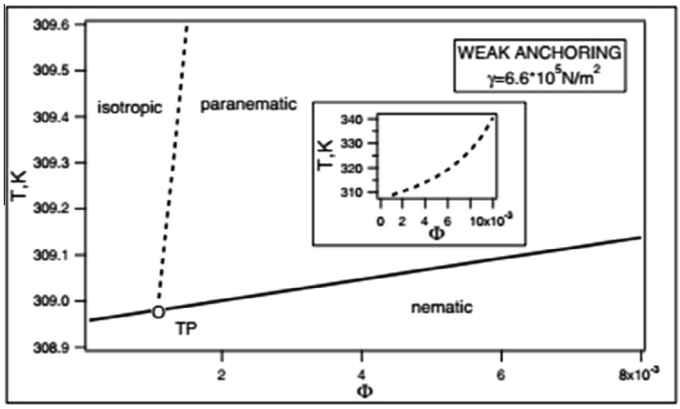

Fig. 8. The (ϕ, T) phase diagram of a homogeneous mixture in the weak anchoring limit [with permission Ref. [180]].

$$f = f_{LC} + f_{CNT} + f_{LC+CNT} + f_C \tag{1}$$

The first two terms in Eq. (1) represent the free energy density of LC and CNT, respectively, while third term is associated with the free energy density of LC/CNT mixture in isotropic phase. The fourth term contributes to the coupling energy. The coupling free energy density is presented in two limiting cases (i) weak anchoring case and (ii) strong anchoring case. Under weak anchoring limit it is considered that anchoring between LC and CNT does not produce any deformation in the nematic ordering. However, under strong anchoring limit, the interaction between CNTs causes topological singularities of the nematic director.

For the homogenous mixing of LC and CNT in weak anchoring limit, the phase diagram as a function of volume fraction is shown in Fig. 8.

The phase diagram can be classified into three regions: (i) isotropic phase, (ii) paranematic phase (where both components have small degree of orientational order) and (iii) nematic phase. For the volume fraction of CNTs $\phi \leqslant 0.00108$ the solid line represents the first order phase transition from nematic to isotropic, whereas, $\phi > 0.00108$ the solid line corresponds to first order transmission from nematic to paranematic phase. The dashed line defines the second order transition from paranematic to isotropic phase. It is also clear from the figure that nematic isotropic phase transition temperature increases with increasing volume fraction of CNT in LC (CNTs act as heterogeneous nucleation agents of LC). The phase behavior is more clear from Fig. 9 where order parameter profile as a function of temperature is shown.

It is clear that for a very small fraction of CNT ($\phi = 1 \times 10^{-3}$) in LC, first order nematic–isotropic transition is observed. However, for $\phi = 3 \times 10^{-3}$ both first order (nematic–paranematic transition at $T \approx 309$ K) and second order transition (paranematic–isotropic transition at $T \approx 312$ K) are observed.

The phase diagram in strong anchoring limit is shown in Fig. 10. The region I in Fig. 10 corresponds to the isotropic phase of both liquid crystal and CNT. Region II belongs to the isotropic phase of LC and ordered phase of CNTs. In region III both components are in nematic phase. For volume fraction $\phi \leqslant 13.5 \times 10^{-3}$, the solid line denotes the first order nematic–isotropic transition. In case of $\phi > 13.5 \times 10^{-3}$ the solid corresponds to first order isotropic–nematic transition of LC and nematic–nematic transition of CNT. It should be pointed out here that order parameter of CNT in mixture is greater in nematic phase than the isotropic phase of LC. The dashed line represents the isotropic–nematic second order phase transition of CNTs in isotropic LC.

In Fig. 11 order parameter as a function of temperature is plotted. A clear first order nematic–isotropic transition at $T = 309$ K is observed for $\phi = 1.0 \times 10^{-2}$. The higher contribution of volume fraction $\phi = 3.0 \times 10^{-2}$ induces first order nematic–isotropic transition of LC and first order nematic–nematic

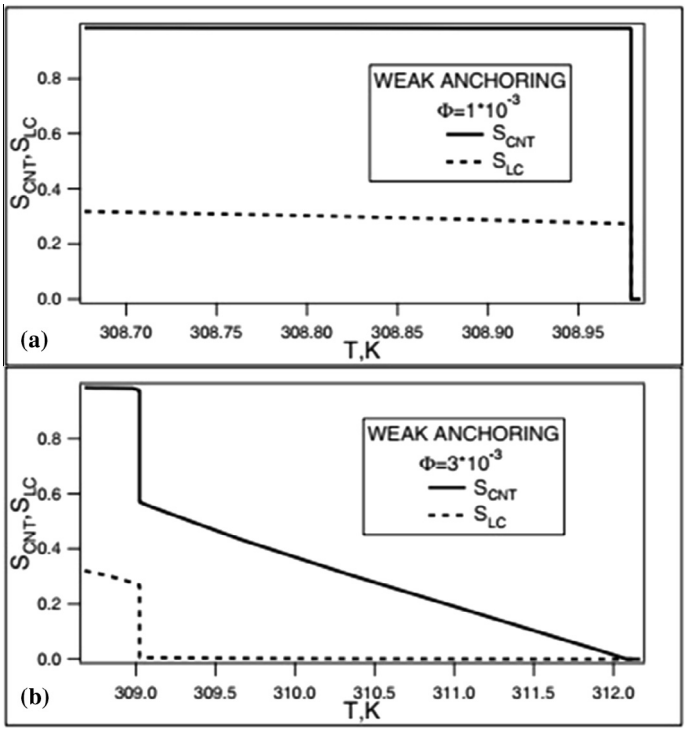

Fig. 9. The order parameter profile of CNTs (continuous line) and LC (dotted line) for $\gamma = 6.6 \times 10^5$ N/m^2 [with permission Ref. [180]].

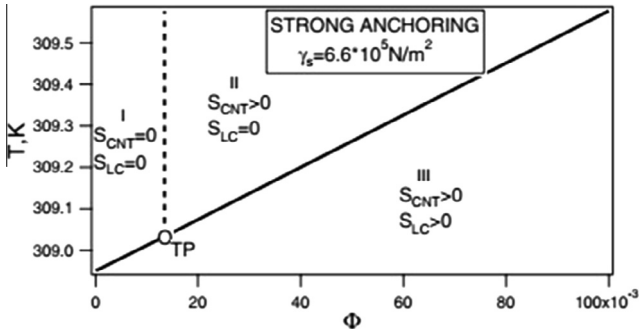

Fig. 10. The (ϕ,T) phase diagram of a homogeneous mixture in the strong anchoring limiting case [with permission Ref. [178]].

transition of CNT at 309.1 K. The jump of order parameter of CNT is small at transition. The phase behavior predicted by Kralj group is in close agreement with experimental results [149,181].

It is predicted that strong anchoring between LC molecules and CNT and highly ordered structure may shift the transition temperature. The incorporation of MWCNTs in a very narrow range of concentration (0.1–0.2%) significantly enhanced the nematic–isotopic (T_{NI}) phase transition temperature [181] observed from DSC, polarized and unpolarized optical microscopy. A chimney type phase diagram is observed. The observed phase transition temperature jumps to ~100 °C when CNT concentration is increased to ~0.1% and it again falls back to ~64 °C when CNT is further increased (beyond

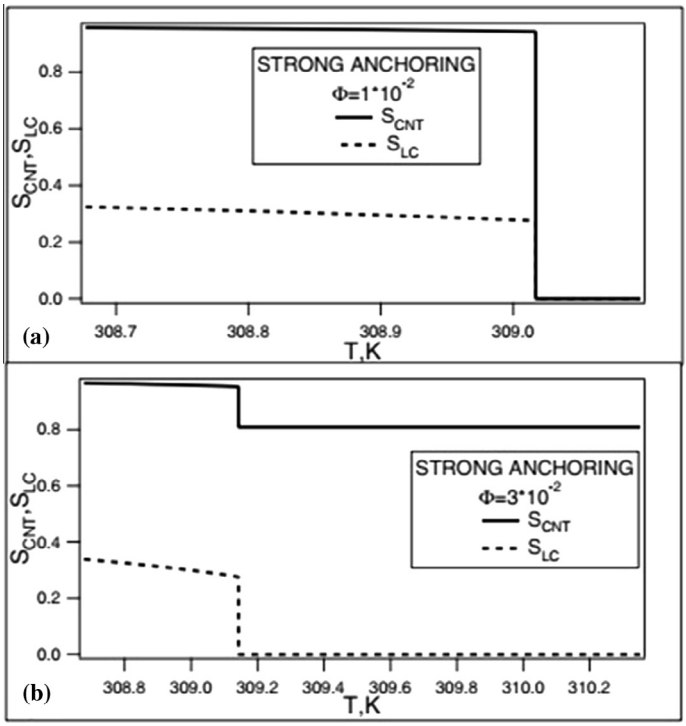

Fig. 11. The order parameters profiles of CNTs (continuous line) and LC (dotted line) for $\gamma = 6.6 \times 10^5$ N/m^2 [with permission Ref. [178]].

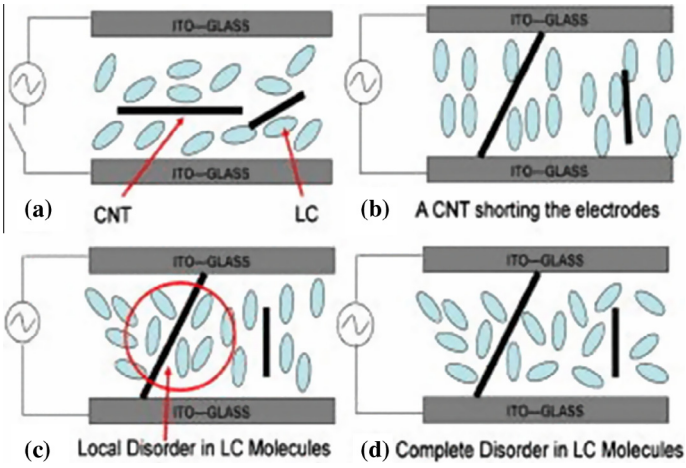

Fig. 12. Schematic of the N–I LC transition under the electric field in presence of annealed nanotubes: (a) initial nematic phase; (b) upon application of electric field across the cell, the CNT rotates out of plane, short circuiting the cell. (c) Local phase transition from N–I occurs close to the shoring CNTs due to Joule heating; (d) the N–I phase transition extends to the whole cell due to diffusion [with permission Ref. [184]].

0.2%). This show there must exist a critical concentration of CNT for the maximum jump of transition temperature. However, C60-Ih/E7 mixture shows a minor decline of 1 °C or less, which is within the experimental error. This indicates that anisotropic shape of CNT plays a crucial role to determine the phase transition of LC/CNT suspension. The mutual alignment of CNT and NLC increases the number of intermolecular association. This anisotropic alignment reduces the entropy of the system and increases the enthalpy. Therefore, phenomenon was treated as entropy driven enthalpy change. Jo et al. and others [172,182] have observed no appreciable change in T_{NI} for both MWCNT and SWCNT doped nematic liquid crystal. A very minute change in transition temperature ~1.10 K has been noticed with very small traces of CNTs (0.0005–0.0060 wt%) in 8CB. However, the transition from I–N and N–SmA remains first order and second order, respectively [183].

A complete phase transition from nematic to isotropic was investigated by Shah et al. [184] in LC/CNT suspension with application of electric field. Below the threshold concentration of CNTs i.e. $c < 0.04$ wt%, only localized isotropic droplet near CNTs were formed. Above the Freedericksz transition threshold, LC and CNT align themselves in the direction of field. The longer CNTs short out the electrodes as shown in Fig. 12. The CNTs provide a conductive path which in turn causes Joules heating. The CNTs work as nucleation site for nematic to isotropic phase transition. As the temperature increases due to Joules heating, the nematic order near CNTs get disturbed first, which appears in the form of bubble around CNTs. Keeping electric field on for some time, temperature of the suspension increases and disorder (bubbles) span throughout the sample.

A recent report by Lebovka et al. [185] shows that DSC peaks appear to be narrower for pristine LC and loaded with small concentration of CNT ($c \sim 0.1$ wt%) for N–I transition at $T_{NI} = 308.5$ K. For large concentration of nanotubes ($c = 1$ wt%) transition temperature shifts to lower side ($T_{NI} = 301.5$ K) and the concerned DSC peak becomes broader. It clearly indicates the destruction of nematic order and highly spatial heterogeneity of the suspension due to presence of NTs. For EBBA + MWCNTs suspension both T_{IN} and T_{NC} were increased by 1 K. However, with increasing concentration of CNT, T_{NI} decreases slightly by 0.5 K, probably due to the agglomeration process resulting in decrease of contact area of MWCNTs and EBBA molecules [145]. Zhao et al. [163] reports that MWCNTs in MPPB acts as inert filler even at higher concentration of NTs. No influence of the admixture of magnetic particles on the temperature of the N–I transition has been observed [186–188].

The concentration dependence of transition temperature is also noticed [141]. It first decreases with functionalized CNT loading of 0.1–0.4 wt% in LC and increases with further increase in loading ($c = 0.5$–1 wt%). The results also indicate that the loading of functionalized MWCNT in LC does not significantly devastate the structure of LC matrix. These results illustrate that MWCNT/LC composite has a better thermal stability and wider mesophase temperature range.

An interesting phenomenon of solidification from LC to solid state (or super cooling behavior) is demonstrated by measuring the electrical conductivity [170]. The super cooled nematic phase was observed at 285–286 K, which is around 20 K lower than the melting points (309 K) for both pure EBBA and MWCNT/EBBA suspension [149,189]. It is noticed that σ initially decreases to a minimum value σ_{min} and then starts increasing with increasing temperature. The reorientation of MWCNT network during the solidification process results in such behavior. The solidification lag time (τ) is found to be dependent on both super-cooling degree (ΔT) and MWCNT concentration. The average time lag can be written as

$$\tau = \tau_\infty \exp\left(\frac{G}{kT}\right) = \tau_\infty \exp\left(\left(\frac{T^*}{\Delta T}\right)^2\right) \tag{2}$$

where G is the critical free energy needed to form stable nuclei, constant τ_∞ and T^* depend on the parameter of nucleating material, concentration of impregnated solid particles and the interface interaction. τ_∞ represents the limiting value of τ for very large ΔT. The decreasing τ and T^* with increasing c reflects the increasing density of crystallization.

According to the photoluminescence spectra shift of 27.2 nm and 10.47 nm is noticed for pure 5CB and 5CB + CNT composite, respectively, in the temperature range 10–297 K. The shift in λ (red shift) is observed due to the conformation change in structure. A very slight change in λ, in presence of NT, reveals the hindrance or strong perturbation to the conformational state of 5CB. The observed

metastable crystalline phase transition $c_1^a \rightarrow c_1^b$ at 230 K is observed in the presence of NTs. It is concluded that NTs partially eliminate some metastable states [185]. Petrov et al. [190] has reported the entrance of new phases in LC/CNT suspension. The pristine 7OBA (*p*-*n*-heptyloxybenzoic acid) LC has phase sequence of I–N–S_c–N_r–C_G–Cry. whereas LC + CNT suspension has phase sequence of I–N–S_c–N_r–C_G–Cry. In the case of 8 μm thick cell, chiral phases appear. The phase sequence of the suspension is I–N^*–S_c^*–N_r^*–S_G–Cry. The reduced cell thickness increases the anchoring strength and lowers the symmetry. This condition is favorable for induced chiral phases. Also the transition temperature of the suspension is lower than the pristine one.

The length bidispersity of CNT in LC under weak anchoring condition is also analyzed [191]. It is found that if (subcritical region) $\gamma_1 < \gamma_c$ (γ is the coupling constant between CNT and LC) the N–I transition is of first order and if (supercritical region) $\gamma_1 > \gamma_c$ the order parameter varies gradually. Also longer tubes are more ordered than the shorter one.

8.2. Optical transmittance, memory effect and hysteresis

The director reorientation in NLC leads to a drastic change in the optical transmittance under the influence of any perturbation. It is now well known that the difference of the optical transmittance (T_0–T, where T_0 is the transmittance for pristine LC cell and T stands for transmittance of LC/CNT suspension) reveals the orientation order of CNT in LC. A well defined step wise change of optical transmittance near nematic to isotropic phase transition is observed [192,193]. T_0–T value is high in nematic phase and substantially lower in isotropic phase. The result clearly indicates a well ordered distribution of CNT in nematic phase of suspension. The recorded T_0–T values are quite different for different LCs. This indicates the different affinity of CNT to different LCs [37,168,170,174]. In Fig. 13, T_0–T values are plotted for 5CB, MBBA/EBBA, ZhK-440 and ZhK806 dispersed with MWCNT for different temperatures.

This system also exhibit nonvolatile memory when system transits from one stable state to another stable state under electric field [194]. However, to initiate this memory, threshold voltage is required below which no irreversibility is observed [40]. A reversible electro-optical response is observed for EBBA doped with CNT ($c < 0.01\%$). However, residual transmittance $T_m > T_0$ for higher concentration of CNT is noticed. The maximum value of M (memory parameter) is observed for $c = 0.02$–0.05 wt% for EBBA + CNT system. MLC6608 + CNT showed a smaller number of pulsations than to EBBA + CNT system, due to smaller value of birefringence. The oscillation generally observed for the optical transmittance curve is caused by the phase incursion higher than $\pi/2$ appearing during the reorientation in an electric field.

The memory efficiency is characterized by memory parameter

$$M = \frac{T_m - T_0}{T_{\max} - T_0} * 100\% \tag{3}$$

where $T_{\max}$ is the maximum value of transmittance.

The maximal memory efficiency are almost similar for ($M = 75$–80%) EBBA + CNT and MLC6608 + CNT series. At the same time, the concentration dependence of M is basically different. The M value first increases rapidly up to the concentration level of $c = 0.02$–0.05 wt% and then starts decreasing with further increase in CNT concentration [38]. A maximum has been observed for EBBA + CNT series at $c \sim 0.02$ wt%, the corresponding curve for MLC6608 + CNT series rapidly grows and saturates at $c \sim 0.1$ wt% [142]. The phenomena of aggregation of CNTs in both LCs are quite different. The formation of dense network of CNTs in EBBA + CNT series strongly increases the sample conductivity. Therefore, the voltage drop across the sample increases which decreases the actual voltage applied to the composite, even below the threshold of memory effect. Also the heating of the sample due to flow of significant current causes the decay of memory parameter in EBBA + CNT composite.

Other reports by Basu and Iannacchione [42,195] indicate the presence of memory in cyano based NLC/CNT suspension. The CNTs imposes short range orientational order to the LC molecules. These pseudo-nematic domains get interacted with the applied external field which results in the reorientation of the NTs and LC molecules. This new oriented structure remains in the deep isotropic phase

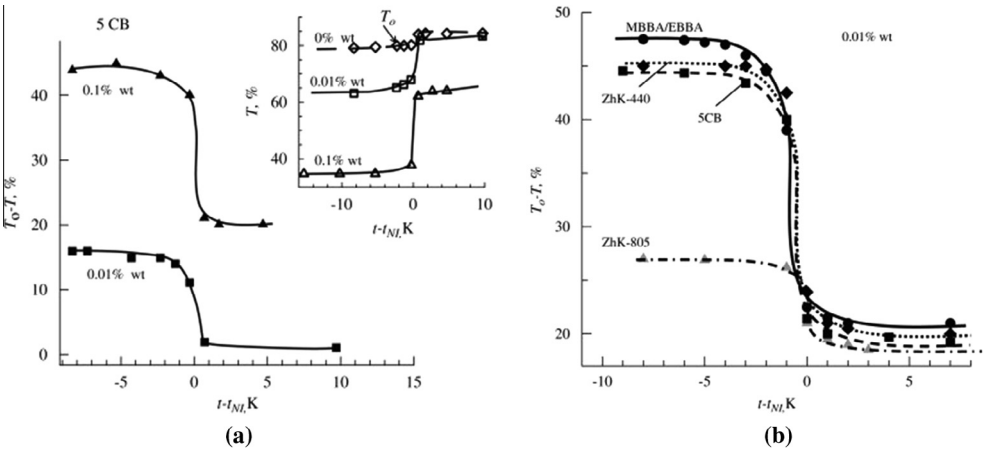

Fig. 13. (a) Difference in transmittance of the nematic matrix 5CB (T_0) and the MWCNT + 5CB composite (T) as a function of relative temperature t–t_{NI}. Inset shows transmittance T versus the value of t–t_{NI}. (b) Difference in transmittance T_0–T for pristine and NT dispersed nematic verses temperature t close to the nematic–isotropic transition point tNI for different LC matrices [with permission Ref. [168]].

even if the external field is turned off, due to absence of any restoring force in isotropic phase. LC/CNT composite revealed the memory parameter of 0.44, which was further enhanced to 0.82 by adding small concentration of chiral dopant (c = 0.1 wt%). The polarization microscopy confirms the continuous planar alignment in LC/Ch/CNT composite. It is argued that twisting forces caused by the chiral agent destroys the local homeotropic alignment state, together with the elastic forces of CNTs, which maintains the planar alignment state formed in an electric field [196].

The observed memory effect in LC/CNT suspension is associated with sustained planar state in the absence of applied field. It is established that incomplete relaxation of LC molecules, after the field is turned off, causes the observed memory effect. The fine network of nanotubes plays an important role in the stabilization of LC planar state. Also the efficiency of suspension considerably depends on the concentration of nanotubes in LC. In other words, the observed memory of the suspension robustly depends on the interaction of nanotubes with LC and with other nanotubes and also on the strength of surface anchoring. With the application of electric field LC molecules reorient from one stable state to another stable state. For U > Uc, the development of EHD in suspension smashes the CNT aggregates and originate some fine nanotube network. This fine network is responsible for the stable planar state even when the field is turned off. The memory mechanism observed is almost similar to the suspension of aerosil, where hydrogen bonding stabilizes the oriented state [197,198].

The observed V–C and V–T curves reveal that hysteresis width of MWCNT dispersed LC are narrower than the pristine and SWCNT dispersed LC [35,199]. Hysteresis width decreases by 35.25% and threshold voltage decreases by 52.5% as compared to pure LC. This reduction in hysteresis width is attributed to the absorption of ions on CNT surface. It is also reported that only trapping of ions is not the cause to decline the hysteresis in a CNT dispersed LC cell [200–202].

8.3. Dielectric and electrical conductivity behavior

Dielectric spectroscopy has been found to be powerful probe to investigate the molecular dynamics of LCs. A large volume of experimental data is also available on the dielectric and electrical conductivity behavior of LC/CNT suspension [27,37,151,168,171,192,203–208]. Lu and Chien [43] have studied the effect of very small trace of CNTs (10^{-3} wt%) in four different LCs (BL006, ZLI4792, MLC6080 and TL204). No change in dielectric anisotropy is found, but increase in imaginary part of dielectric permittivity indicates the increase in conductivity of the material.

A dielectric study in a wide frequency range is carried out by Kovalchuk et al. [36] with varying concentration of CNTs (0–0.25 wt%). Fig. 14 shows the variation of dielectric permittivity and loss behavior as a function of frequency for pure E7 and dispersed E7 with MWCNTs [209]. In low frequency range (10^{-2}–10 Hz), drastic increase in ε'', due to participation of CNTs in charge transfer mechanism (through electron exchange between electrodes and ions) has been observed. Also CNTs shunt the double electric layer, suppressing the field screening effect. At lower concentration of CNTs ($c < 0.05$ wt%), the charge transfer is through LC material, but for concentration $0.05 < c < 0.25$ wt%, the shunting of electric double layer is effective.

In the mid frequency range (10–10^5 Hz) σ_{AC} is found to be almost independent of applied frequency, when $c \leqslant 0.025$ wt% but for $c > 0.025$ wt%, σ_{AC} is found to be a function of f as

$$\sigma_{AC} = \sigma_i + S f_n^m \tag{4}$$

where σ_i is the ionic conductivity, S and m are the constants and f_n is the normalized frequency. m increases rapidly when $c > 0.025$ wt%, indicating the conductivity transition from ionic to electronic one. The observed transition is accounted for formation of continuous networks of CNTs. In high frequency range (10^5–10^6), the dielectric spectra follow the Debye Law, for $c \leqslant 0.05$ wt%. The relaxation time increases with the dispersion of CNTs, suggesting the strong interaction between CNTs and LCs. The conductive behavior of EBBA/MWCNT composite as function of CNTs concentration is shown in Fig. 15.

For an applied voltage greater than 10 V, Lisetski reports [168] increase of σ with applied voltage for different NLC + CNTs dispersion, accounting for direct reorientation of NTs structure, without direct intermediation of the nematic matrix. Even though the reorganization of NTs can be accompanied with the damage of conductive path, but at the same time formation of thick aligned percolative columns between the electrodes enhances the electrical conductivity. However, electrical transport accelerates through the mechanism of hopping or tunneling at $U > 10$ V.

The observed σ curve for EBBA + CNT dispersed series increases monotonically, then saturates at the concentrations of 0.03–0.05 wt% [146]. Such change in growth rate is due to the achievement of the percolation threshold, where 3D network formed becomes a conductive path for the charge transportation. The electrical conductivity depends on the concentration of CNTs $c \sim 0.01$–0.1 wt% in LC + CNT suspension [193]. A similar result has also been reported by Zhao et al. [163]. They reported that surface resistance of the 8% MWCNT/MPPB suspension decreases by 7 orders of magnitude. Up to the

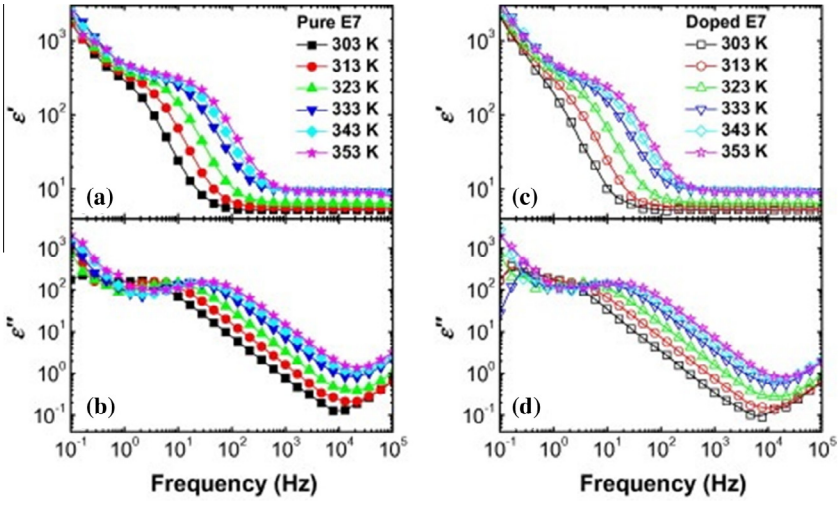

Fig. 14. (a) Real part and (b) imaginary part of dielectric complex curves of pure E7 at various temperatures. (c) Real and (d) imaginary part of complex curves of CNT doped E7 at various temperature [with permission Ref. [209]].

electrical percolation concentration, the surface resistivity decreases markedly but beyond this concentration it decreases slowly. Beyond the percolation concentration, with increasing number of CNTs, the distance between them will decrease, which results in the decrease of the resistance of hopping.

In the isotropic phase of LC + CNT suspension, the suspension show increment in $\bar{\varepsilon}$ with increasing applied voltage [195]. The observed behavior is attributed to the presence of pseudonematic domains (PND). A schematic view of the formation of pseudonematic domains is shown in Fig. 16. The thermal energy ($\sim 10^{-2}$ eV) is found not to be so strong to break the anchoring between CNT and LC ($\sim$20 eV) molecules. This strong interaction leads to the short range ordered structure surrounding the CNT, having director along tube axis. This local pseudonematic domains directly interacts with the applied external field, which results in increment of $\bar{\varepsilon}$. It should be pointed out here that the system does not relax back to its previous position after the field is turned off. Due to absence of elastic interaction in isotropic LC medium, there is no restoring force to turn back these pseudonematic domains and therefore, domains remains oriented. That is why these systems shows large hysteresis in isotropic phase which is absent in pure LC [realization of non volatile electromechanical memory effect].

Transition from conducting to non conducting state is noticed for a very low concentration of MWCNT (C = 0.1 wt%) in EBBA [149]. This highly conductive state is associated with the conductive path formation inside the nematic matrix (above percolation threshold). A more interesting result is observed under heating–cooling cycle. During heating cycle σ initially decreases drastically in the vicinity of S–N transition and then it becomes increasing function of temperature as plotted in Fig. 17. Similar results were also observed during the cooling cycle at N–S transition. The observed behavior was explained on the basis of thermal expansion of the host matrix. This thermal expansion results in breaking of continuous network and therefore, σ decreases rapidly.

Above S_A–N transition, the increase in σ with varying temperature is associated with the increase in the number of hopping junction due to Brownian motion intensification. Above the percolation threshold network formation of CNTs weakens the temperature effect. The hysteric behavior is found to be more pronounced around percolation threshold. The activation energy for thermal fluctuation can be written as [36,149]

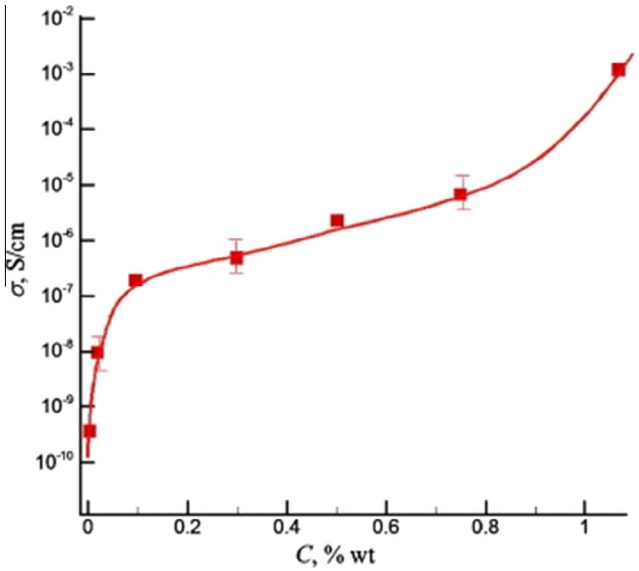

Fig. 15. Electrical conductivity σ versus weight fraction of nanotubes C (%) in MWCNTs/EBBA composites, T = 313 K, f = 1 kHz, U = 1 V [with permission Ref. [149]].

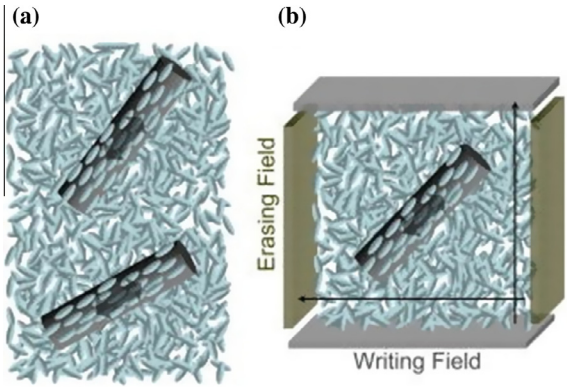

Fig. 16. Schematic diagrams: (a) field responsive anisotropic pseudonematic domains due to LC (ellipsoidal)-CNT (cylindrical) interaction in the isotropic media; (b) a model for a four electrode writing and erasing memory [with permission Ref. [195]].

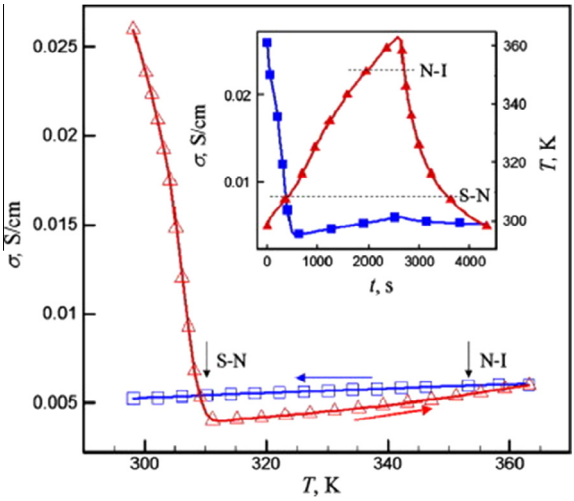

Fig. 17. Electrical conductivity σ versus temperature T, c = 1 wt%, f = 1 kHz, U = 1 V. Inset shows electrical conductivity σ and temperature T evolution with time t [with permission Ref. [149]].

$$\sigma \propto e^{\left(-\frac{W}{k(T+T_0)}\right)} \tag{5}$$

where w denotes the energy required for crossing of the insulator gap between conductive clusters by an electron and T_0 is the limiting temperature above which the thermal activated conduction occurs. The activation energy calculated from the above relationship follows the decreasing trend with increasing concentration of MWCNTs in EBBA.

Jayalakshmi et al. and others [210,211] observed that only reorientation of CNTs cannot be the cause for observed large increase in conductivity, especially in the case where the cell gap is much larger than the CNTs length. The increase in σ is four orders of magnitude (above 8 V) with increase in applied electric field, but observed increase in σ with increasing magnetic field is merely by a factor of two. The current voltage curve, points out toward the dielectric breakdown situation (abrupt increase in electrical conductivity beyond certain voltage). This dielectric breakdown also causes local heating effect in system. Steady increase in temperature due to local heating is given by

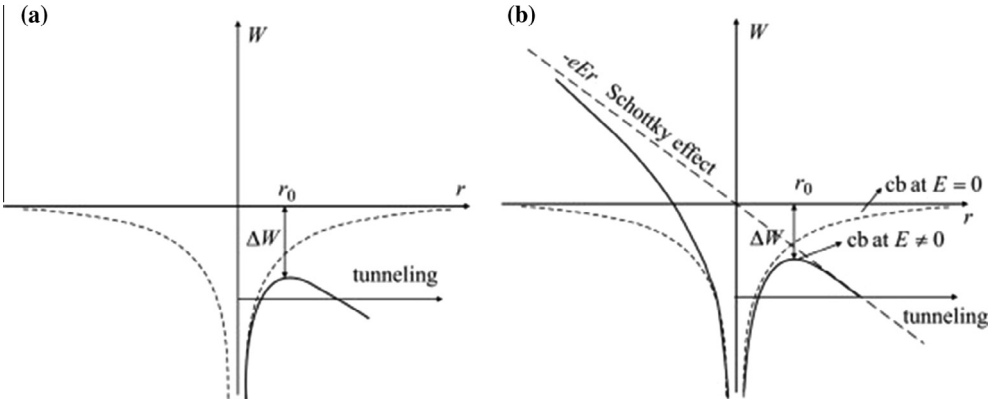

Fig. 18. Schematic diagram illustrating the Poole–Frenkel effect in (a) dielectric; (b) dielectric doped with semiconductive impurities (cb – conduction band) [with permission Ref. [212]].

$$\Delta T = \frac{\pi f \epsilon_o \epsilon^i U^2}{2kd}\left(1 + \frac{kL}{G}\right) \tag{6}$$

where ϵ_o is the permittivity of free space, d the sample thickness, k the heat transfer coefficient, G the thermal conductivity, L the thickness of glass plate, f the frequency of applied field and U is the amplitude of applied voltage. Calculation based on above model, for 8CB + 0.05 CNT, results in an increase of ΔT by ~10 K, for an applied voltage of 7 V. This large increase in local temperature might drive the N phase to isotropic phase. Therefore, dielectric breakdown and local heating effects also play an important role.

The effect of positive temperature coefficient on σ was manifested by Goncharuk and workers [159]. The observed phenomenon was explained on the basis of thermal expansion of LC molecules. Thermal expansion of LC molecules breaks the network which results in decrease of electrical conductivity. It should be noted here that most differentiable effect was observed for the percolation threshold.

Cirtoaje et al. [212] has explained the conductivity behavior on the basis of Poole–Frenkel effect. A schematic visualization for this effect is drawn in Fig. 18. In the case of planar aligned cell the current density can be written as

$$J = \left(N_{eff} N_c\right)^{1/2} E^{3/2} \exp\left[-\frac{\epsilon_D}{2kT}\right] \exp\left[\frac{e^{3/2} E^{1/2}}{\left(4\pi\varepsilon_0\varepsilon_r\right)^{1/2} kT}\right] \tag{7}$$

$N_{eff} \rightarrow$ effective carrier concentration inside conduction band,
$\epsilon_D \rightarrow$ energy of donor level,
$N_c \rightarrow$ concentration of states in conduction band.

Carbon nanotube behaving as n-type semiconductor contributes to the extrinsic part of conductivity. The electron placed at donor level (activation energy for donor level $\epsilon_D = 0.01$ eV) are responsible for such conductivity. However, at a given temperature and electric field when donor level becomes empty, only intrinsic part contributes to the conductivity.

San et al. [41] reported that dielectric anisotropy ($\Delta\varepsilon$) is found to be less ($\Delta\varepsilon = 12$) for E7 + SWCNT as compared to E7 + MWCNT ($\Delta\varepsilon = 22$) and E7 ($\Delta\varepsilon = 35$), indicating a more ordered structure. In another report it was observed that there exist conductive paths due to directionally aligned CNTs aggregation after some critical electric field has been applied. CNTs move toward anode and agglomerate there, so that correlation length decreases. This facilitates the electron transfer and produces high conductivity and dielectric loss [213].

The dielectric anisotropy $\Delta\varepsilon_{LC+CNT}$ can be given as [214]

$$\Delta\varepsilon_{LC+CNT} = \rho_{LC}\Delta\varepsilon_{LC} + \rho_{CNT}\Delta\varepsilon_{CNT} + \Sigma\Delta\varepsilon_{PND} \tag{8}$$

where $\Delta\varepsilon_{PND}$ is the dielectric anisotropy of local PND. Substituting typical values for ρ_{LC}, ρ_{CNT}, $\Delta\varepsilon_{LC}$, $\Delta\varepsilon_{CNT}$ $\Sigma\Delta\varepsilon_{PND}$ contributes 20% of the total value of $\Delta\varepsilon_{LC+CNT}$.

In spite of large enhancement in dielectric permittivity in both N and isotropic phase the dielectric anisotropy of the composite system decreases [215]. The results are quite interesting as compared to the behavior with strongly polar LC. It is argued that weakly polar PCPBB molecule has different interaction with CNT. PCPBB molecule rather prefers perpendicular alignment on CNT surface due to presence of hydrophobic forces.

Theoretically to address the behavior of dielectric permittivity of NLC/CNT suspension, Fuh and workers [216] carried out modeling using Maxwell–Garnett theory. CNTs are treated as conductive or lossy dielectric materials. The volume fraction of CNT is kept low to ignore the CNT interaction. The CNTs are approximated by ellipsoids with its major axis $c \gg a, b$ (minor axis). It is also considered that CNTs are well aligned along nematic director. Under the two cases considered the effective dielectric permittivity is given as:

Case [i] below the Freedericksz transition (director in y direction)

$$\overline{\overline{\varepsilon_{eff\_nem}}} = \begin{vmatrix} \varepsilon_{eff\_x} & 0 & 0 \\ 0 & \varepsilon_{eff\_y} & 0 \\ 0 & 0 & \varepsilon_{eff\_z} \end{vmatrix} = \begin{vmatrix} \varepsilon_{eff\_\perp} & 0 & 0 \\ 0 & \varepsilon_{eff\_\parallel} & 0 \\ 0 & 0 & \varepsilon_{eff\_\perp} \end{vmatrix} \tag{9}$$

Case [ii] above Freedericksz transition threshold (director in z direction)

$$\overline{\overline{\varepsilon_{eff\_nem}}} = \begin{vmatrix} \varepsilon_{eff\_x} & 0 & 0 \\ 0 & \varepsilon_{eff\_y} & 0 \\ 0 & 0 & \varepsilon_{eff\_z} \end{vmatrix} = \begin{vmatrix} \varepsilon_{eff\_\perp} & 0 & 0 \\ 0 & \varepsilon_{eff\_\perp} & 0 \\ 0 & 0 & \varepsilon_{eff\_\parallel} \end{vmatrix} \tag{10}$$

In case or isotropic NLC/CNT suspension (not considering the pseudonematic domains) the effective dielectric permittivity can be given as [177]

$$\overline{\overline{\varepsilon_{eff\_iso}}} = \varepsilon_{lc}\bar{\bar{I}} + f\varepsilon_{lc}\left[\frac{\overline{\overline{\varepsilon_{cnt}}} - \varepsilon_{lc}\bar{\bar{I}}}{\varepsilon_{lc}\bar{\bar{I}} + (1-f)\bar{\bar{N}}(\overline{\overline{\varepsilon_{cnt}}} - \varepsilon_{lc}\bar{\bar{I}})}\right] \tag{11}$$

where ε_{lc} should be taken as $\varepsilon_{lc} = \frac{\varepsilon_{\parallel}+2\varepsilon_{\perp}}{3}$.

It is found that the enhancement of dielectric anisotropy of the nematic liquid crystal is governed by the dipolar orientation of CNT. It should also be noticed here that effective dielectric anisotropy vs. volume fraction of CNTs in NLC curve reveals that there exist turning point where $\Delta\varepsilon$ starts decreasing with increasing concentration of CNT. This turning point is attributed to the limitation of MG approximation or large bundles of CNTs are formed.

8.4. Switching mechanism and ionic effect

The electro-optical effects in LCs originate from the reorientation of the director in the macroscopic volume under the influence of external perturbation. The visco-elastic properties and initial orientation play an important role to decide the behavior of dynamical processes. A certain amount of energy is required to initiate the director reorientation. Under the homogenous alignment of liquid crystal molecules, the applied field tries to align the director along the field direction. For fields well below a certain voltage, the liquid crystal molecules remain in its homogenous position. As the strength of field is increased deformation occurs and it increases with increasing field. This deformation is known as Freedericksz transition. The study of Freedericksz transition is important to the operation of liquid crystal displays [52] because deformation causes a dramatic change in the optical characteristics.

In recent years, a number of research papers have been published emphasizing on the effect of dispersion of CNTs on Freedericksz transition in LCs in terms of switching time and threshold voltage.

Kaya et al. [172] noticed that threshold voltage obtained for LCs dispersed with dye and nanotube is lower than those of solely dye dispersed ones. This decrease may be attributed to the suppression of the field screening and increase of the dielectric anisotropy by the addition of nanotubes. After dispersion of CNTs in LC, response time has been improved as reported [43,137,217–223]. The improvement in response time (specially decrease in fall time) is attributed to the change in anchoring energy by an order and the effect is dominated by the applied voltage (warm up voltage). τ_{fall} in case of OCB cell may be given as (ignoring the flow effect)

$$\tau_{fall} = \frac{\gamma_1}{\varepsilon_o|\Delta\epsilon|V_b^2 - \pi^2\kappa}\left(d^2 + \frac{4d\kappa}{W}\right) \tag{12}$$

where γ_1 is the rotational viscosity, k the effective elastic constant, W is anchoring energy, V_b is warm up voltage and all other symbols have their usual meanings. The increase in anchoring energy is due to the π–π stacking between CNT surface alignment layers and LC molecules. A slightly higher threshold voltage for E7 + MWCNT suspension is noticed, owing to increased effective elastic constant and increased anchoring strength at the alignment layer. Even ultrapure SWCNT introduces some impurities to the host, which results in the increase of electrical conductivity below Freedericksz transition. Above Freedericksz transition, the reorientation of CNT from planar to homeotropic alignment increases the electric conductivity [224]. However, the threshold voltage differs by 0.5 V for ac and dc excitation [221].

The twist elastic constant K_{22} in the CNT dispersed LC is increased by ~5.5%. The reaction time in terms of rising and decaying is improved by dispersing CNT [34,222]. An improvement of almost 18% in decay time is noticed.

It is clearly observed that with increasing concentration of CNTs in E7, the rotational viscosity decreases. The experimental result also suggests that there exist an optimum concentration of CNTs in LC which permits the enhancement of electro-optical properties. The change in rotational viscosity is associated with the different torque experienced by the CNT and LC molecules and with the change in order parameter [137].

Effect of carbon nanotubes length on the electro-optical properties of LC dispersed with CNT is studied by Lee et al. [225]. The operating voltage comes out to be (3.19 and 3.24 V for LC + CNT mixture of 290 nm and 177 nm tube length, respectively) higher than the pure LC, which is associated with the increase in twist elastic constant (K_{22}), due to strong interaction between CNT and LC molecules. However, no appreciable change in rise time was observed with CNT length variation but decay time for LC + CNT composite is lower than pure LC. Also shorter tube length has faster response to decay than longer tubes. Basu et al. found that in 5CB + CNT composite, the elastic constant of LC + CNT composite is 1.21 times that of LC [195]. It is also demonstrated that alignment layer has also significant effect on the electro-optical properties of CNT/LC suspension. DMOAP ([(3-trimethoxysilyl)propyl] octadecyldimethylammonium chloride as an alignment layer increase the V_{th} whereas it almost remains unaltered for cell having polyamide as an alignment layer, with increasing CNT concentration [226].

In the case of NLC loaded with magnetic CNTs for a very weak magnetic field of H = 20 mT, colloids results in phase retardation of $\Delta\phi$ = 0.59 rad [177]. Dependence of $\Delta\phi$ on H can be divided into two region. For $H < H_{FR}$ a threshold less monotonic increase of phase retardation was observed. For $H > H_{FR}$ the sharp reorientation of the director occurs. This magnetically induced phase retardation increases with increasing concentration of ferromagnetic particles. However, no change in H_{FR} was noticed with varying concentration of NTs.

It is clearly observed that behavior of 6CHBT dispersed with SWCNT does not differ significantly from the pristine 6CHBT. However, strong influence of magnetic nanoparticles is noticed. The experimental finding showed a strong shift of the critical voltage, due to presence of Fe_3O_4 particles because magnetic particles hinder the reorientation of the director of liquid crystal by the electric field. The calculated anchoring energy for 6CHBT + SWCNT and 6CHBT + SWCNT/Fe_3O_4 vary within the range of 1.1×10^{-3}–8.8×10^{-3} N/m and 5.5×10^{-2}–15.1×10^{-2} N/m, respectively [186]. Similar results were also observed for 6CHBT + MWCNT/Fe_3O_4 [187].

The presence of ions in LC degrades the performance of LC devices. The ions are adsorbed on the surface of alignment layer and generate an internal field. As a consequence, problem of image sticking

and increased operating voltage take place. Recently it has been realized that CNTs are effective in suppressing the screening effect in LCs via the adsorption of ions [35,44,45,227]. Voltage holding ratio (VHR) for E7 + MWCNT composite is found to increase from 48% to 61%. The time evolved VHR measurements indicates a life span of 118 h for doped cell as compared to 59 h for pure E7. Also doping a small 0.050 wt% trace of CNT in E7, significantly trapped the mobile ions, which reduces the space charge polarization, decreasing ε' in low frequency region [228]. The CNTs are effective in polarizing mobile ions in NLC [229].

When undesired impurity ions are excessive in liquid crystals, the ion charge effect on the orientation of liquid crystals will be reduced to an offset value. The voltage offset caused by the ion-charge effect can be modified from [44]

$$V_{offset} = (1-k)\frac{2nqd_{LC}d_{AL}}{2d_{AL}\varepsilon_{LC} + \varepsilon_{AL}d_{LC}} \tag{13}$$

where k is the ion trapping coefficient, q the elementary charge, n represents the ion charge density, d_{LC} and ε_{LC} stand for thickness and dielectric permittivity of the liquid crystal layer and d_{AL} and ε_{AL} are the thickness and dielectric permittivity of the alignment layers. $k = 1$ stands for the best ion trapping capacity of carbon nanomaterials. The ion trapping coefficient ~0.343 was noted down for long MWCNT in E7 [195]. Longer CNT are found to be more effective to reduce the ionic effect due to large surface area and high aspect ratio. CNT plays significant role in suppressing the nematic backflow effect [230].

In another report the ionic concentration in E7 + CNT suspension is found to be lower as compared to the pristine counterpart [209]. At some higher temperature ion concentration almost becomes equivalent. The CNT effectively trap the ion at lower temperature. As the temperature is increased due to gain in the kinetic energy, ions depart from the CNT surface. Also diffusion constant is reduced by ~45% by the insertion of MWCNT. This indicates that CNT not only adsorb the ionic impurity at its surface but also effectively hinder the ion transport. Chen et al. [231] also reports the suppression of field screening in NLCs by CNTs. The transient current peak behavior is expressed as $I_P \propto V^{\alpha}$, where α is found to be 1.3 and 1.6 for pristine E7 and E7 + CNT, respectively. It is clear that peak current is higher in E7 and lower for E7 + MWCNTs, indicating toward the adsorption of charge density. The maximum voltage drop in the electric bilayer is given as

$$V_d = \frac{2L_d\sigma}{\epsilon_o\Delta\epsilon} \tag{14}$$

The V_d observed for E7 (0.55 V) is higher than that of E7/MWCNT suspension (0.35 V), which confirms that CNTs suppresses the field screening effect [204,231]. In twisted nematic liquid crystal cell Jo et al. [182] reported no appreciable change in VHR for both MWCNT and SWCNT dispersed NLC.

The switching mechanism of LC based devices is governed by the visco-elastic coefficient. Both rotational viscosity and elastic constants are found to be lower for LC/CNT suspension. Two possible causes for the decline in rotational viscosity are associated with the decrease in order parameter and incoherent response of suspension. However, at low concentration of CNTs in LC the change in order parameter can be neglected. With the application of field both CNT and LC try to align along the field direction. The electric torque experienced by CNT and LC are quite different from each other as both have different aspect ratio and dielectric anisotropy. This asymmetrical behavior of LCs and CNTs in suspension demises the collective behavior of the suspension, which results in the form of decreased rotation viscosity. The reported decrease in threshold voltage of the suspension is associated with the suppression of field screening and increase in dielectric anisotropy with the insertion of nanotubes. MWCNT and SWCNT have different ion trapping coefficient due to their structural and diverse electrical properties. Also longer nanotubes are found to be more effective to reduce the ionic effect [199].

8.5. Diffraction efficiency

The field induced reorientation of LC director due to coupling of dielectric anisotropy with field results in the variation of refractive index, which make NLCs as potential photorefractive materials.

This photo-refractivity is further enhanced by loading of CNT in NLC. In Raman Nath regime a photorefractive gain of 10^3 cm^{-1} has been achieved [232,233] and it depends on the external applied field, pump/probe intensity ratio and total input intensity. However, the gain is limited by cell gap due to increased elastic energy, as no gain has been observed for grating spacing smaller than 5 μm. Another work by Lee and Hsiao [234,235] reveals that diffraction efficiency varies in phase with the electric field pulse of <0.5 Hz. Also it is found that grating can be made hidden or it can be retrieved by a continuous driving voltage or pulse application. Persistence grating is achieved for a beam intensity of 1.2 W/cm^2 and total illumination time of 20 min [33]. The accumulation of CNT in the form of grooves traps the space charge effectively, which results in the form of internal electric field. This induced electric field modulates the LC director, which results in the form of grating.

The study of the temporal holographic grating induced by the interference modulation of pulse train of two coherent beams, with the application of dc field, reveals that diffraction efficiency and decay time strongly depends on the pulse width of optical excitation [235]. The surface charge assisted grating decays slowly and survives for the next writing beam which results in more intensity to the grating. This temporal superposition of the optical excitation are additive in nature.

Diffraction efficiency of 6.5% and 5.5% for E7/0.05 wt% SWCNT and E7/0.05 wt% MWCNT, respectively, is achieved by San and coworkers [41] as compared to 2% for pure E7. An increment of ~1.8 times in the diffraction efficiency has been found [236]. The maximum diffraction efficiency of 5.8% for the cell containing 0.8% MR dye and 0.002% CNTs has been noticed as compared to the 3.2% for the same cell without CNTs. The diffraction efficiency of around 45% is achieved for E7 + MR + CNT suspension [221,237]. A first order diffraction efficiency η = 8% is obtained for a sample with absorption constant α = 4 cm^{-1} and a beam power of 2 mW/cm^2 [500 μW, 5 mm beam diameter] in NLC + SWCNT suspension. Also very high value of effective non linear index coefficient η_2 = 0.8 cm^2/W was estimated. This enhanced response is due to combination of higher photorefractive response of SWCNT and the higher DC voltage that these samples can hold before dynamic scattering sets in [238,239].

The optical reorientation of SWCNT in E7 using MR dye has been observed via trans–cis photomerization of dye [41] in E7 + MR + SWCNT suspension system. The reorientation of SWCNT is noticed around 10 mW laser power, which reflects in the form of increase in photocurrent clearly reflects the reorientation of the nanotubes.

9. Influence of electric/magnetic field in NLC + CNT composite and electro-hydrodynamic flow

The results discussed above do not consider the motion of CNTs in LC. However, it is expected that CNTs must have translational motion under the influence of electric field due to their large induced polarization along the tube length. Recently, the translational motion of CNTs under application of sufficient electric field has been reported [154]. Optical micrographs for pristine LC and SWCNT/LC composite for various applied voltage is shown in Fig. 19. At low frequency of 1 Hz CNT experiences repulsive and attractive forces and results into and fro motion between the electrodes. But at some high frequency ~60 Hz, the change is so quick that translation starts at one electrode but cannot reach the opposite electrode. The deformation of the LC director is generated along the moving direction of tubes which appears in the form of bright vertical stripes under crossed polarized condition. However, the requirement for this translational motion is that CNT must have permanent dipole moment because induced dipole moment originates only the reorientation of tubes along the field direction. The translational motion of the CNTs has also been observed in OCB cell at 10 V with a frequency of 5 Hz [240]. The translation motion of CNT is attributed to the ion adsorption efficiency of CNT. The trapped impurity ions make the CNT charged, which appears in the form of squirmed motion under the application of electric field.

The pattern dynamics of translational motion of CNTs in LC media under the application of sufficient ac and dc fields is well explained by Jeong et al. [153]. In a homeotropically aligned cell when a sufficient ac field (60 V, 60 Hz) is applied, four lobe patterns were clearly visible through polarizing optical micrograph. Similar mechanism are also observed for homogeneously aligned cell driven by the in plane field.

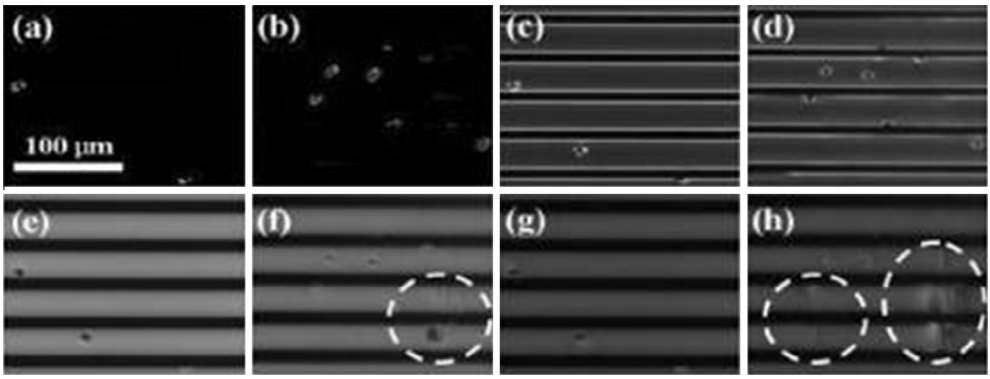

Fig. 19. Optical microphotographs of the cells with the LC only and SWCNT-doped LC cell, when the applied voltages were 0 V_{rms} [(a) and (b)], 10 V_{rms} [(c) and (d)], 60 V_{rms} [(e) and (f)], and 120 V_{rms} [(g) and (h)], respectively [with permission Ref. [154]].

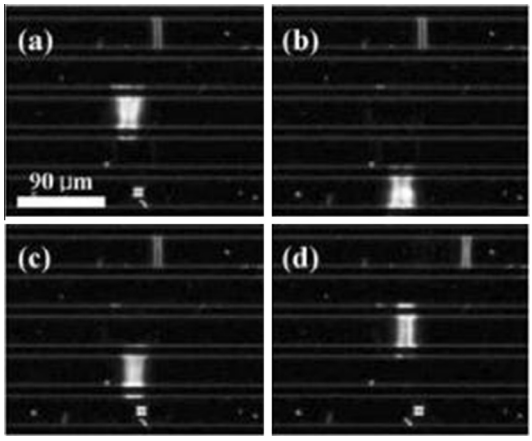

Fig. 20. Optical microphotographs of the SWCNT-doped LC cell at 120 V_{rms} as a function of the angles between the crossed polarizers and the rubbing direction parallel to the in-plane field direction: (a) 0°, (b) 30°, (c) 60°, and (d) 90° [with permission Ref. [154]].

The translational motion of CNT under the action of applied field induces distortion to the LC director. This phase retardation of the LC medium appears in the form of four lobe pattern [241]. The observed pattern is shown in Fig. 20. At low electric field, the translational motion of CNT starts with low velocity and amplitude, which produces very undersized deformation to LC director. Therefore, some indistinct textures are observed. However, at some high electric field (>160 V) CNT moves very fast between the electrodes and produces large deformation to the LC director, which appears in the form of four lobe texture. In the intermediate range of electric field (120–160 V) CNTs are not able to reach one of the electrode, it return back in between during the negative half cycle. The superposition of these two pressure waves (one during upward motion and another during downward motion) results in twin director, which finally appears in the form of ring around four lobes.

The influence of dielectrophoresis forces (DEP), which drives the dynamics of CNT in LC medium under the action of electric field, is reported well by Srivastava and workers [242]. The origin of DEP forces were related with large induced dipole moment in the CNTs due to their high aspect ratio in the presence of electric field. Ignoring the DEP forces CNT can be written as

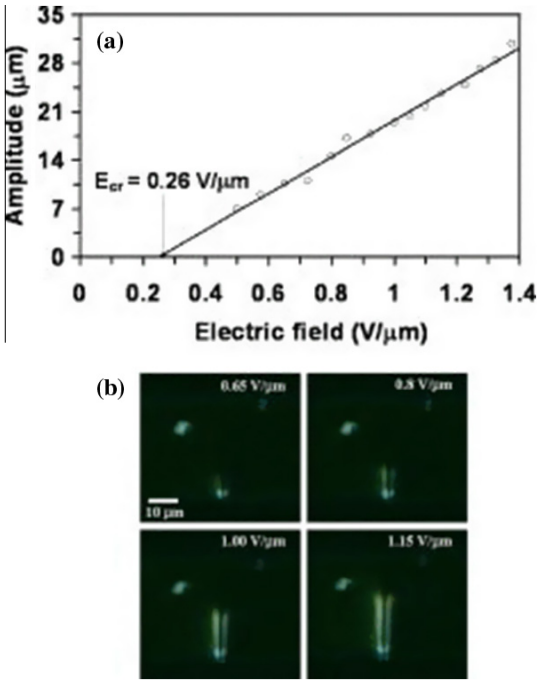

Fig. 21. (a) Amplitude of translation motion of CNTs vs. electric field at the frequency of 60 Hz, for homogenously aligned cell driven by in plane field. (b) Optical micrographs of the SWCNT doped LC cell describing the amplitude of the translation motion of CNTs at different field of 0.65, 0.80, 1.0 and 1.15 V/μm at the frequency of 60 Hz in the homogenously aligned cell driven by in plane field [with permission Ref. [242]].

$$F_{DEP} = \Gamma \varepsilon_m Re\{K(\varepsilon^*_{CNT}, \varepsilon^*_m)\} \nabla E^2 \tag{15}$$

where $\Gamma = \frac{\pi r^2 l}{6}$, Γ is a geometrical factor and ε^*_{CNT} and ε^*_m are the complex dielectric permittivity of nanotubes and LC, respectively. K represents the complex polarization factor and E denotes the applied field. The DEP force tries to move the CNT in LC medium toward one of the electrode. Considering the displacement in x direction, the equation can be written as

$$x = \frac{\frac{(E_O - E_{cr})}{\omega}\sqrt{2\Gamma \varepsilon_m Re\{K(\varepsilon^*_{CNT}, \varepsilon^*_m\}}}{\sqrt{m}}[1 - \cos(\omega t)] \tag{16}$$

E_O denotes the applied ac field and E_{cr} is defined as critical field. The amplitude or maximum displacement can be written as

$$x_{\max} = \frac{\frac{2(E_O - E_{cr})}{\omega}\sqrt{2\Gamma \varepsilon_m Re\{K(\varepsilon^*_{CNT}, \varepsilon^*_m\}}}{\sqrt{m}} \tag{17}$$

The theoretical predictions were well satisfied by the experimental finding on super fluorinated LC mixture dispersed with 0.005 wt% SWCNT. The amplitude of translation motion of CNTs in LC/CNT composite for different strength of applied electric field is shown in Fig. 21. The light leakage in the form of vertical strips is observed in homogenously aligned cell, which moves back and forth between the electrodes driven by in plane field.

It was also observed that amplitude of the translational motion of CNTs between electrodes decreased with increasing frequency at a constant voltage, but it increases with increasing electric field at a constant frequency.

In nematic liquid crystals, with the application of electric field (above a certain voltage) a periodic variation of the director orientation and hydrodynamic flow results in electrohydrodynamic instability. This could be visualized as a periodic pattern of domains. These domains, in general, are known as Kapustin–William domains. Black and white stripes appear on screen. These stripes are caused by the periodicity of the change in the refractive index for an extraordinary ray due to variation in the director. The Kapustin–William domains are aligned perpendicular to the director. Recently, the effect of CNTs on this EHD instability been studied thoroughly.

With a small concentration of CNT in EBBA, $c < 0.002$ wt% and an applied voltage of $U = 10$ V, reorientation from homeotropic to planar state occurs [38]. At $U = 80$ V, EHD instabilities appears. It appears in the form of Kapustin–William domains between $U = 80$–110 V and it becomes turbulent at $U > 120$ V. System returns to its initial state after field is switched off. For higher concentration of CNT $c = 0.02$–0.05 wt%, these EHD instabilities appears at very low applied Voltage $U = 15$ V. Initially these flows appear in the vicinity of aggregates. With increasing voltage, EHD flow intensity increases and captures almost the whole available area. This flow disintegrates the aggregates and improves the CNT dispersion and the number of planar stable states (due to stable CNT network) increases in the cell, which appears in the form of bright state under crossed polarized condition. The stable states exist even after the field is turned off. The EHD is also observed for $c > 0.02$ wt%, but planar states does not remain stable and it returns to initial state after the field is removed. The formation of this stable state is crosschecked by the conductivity measurement. The current flows through this continuous network (for $c > 0.05$ wt%). Different optical texture demonstrating the changes in structure under various applied electric field is shown in Fig. 22. The observed phenomenon due to involvement of CNT is further confirmed by another experiment on EBBA + CNT composite using polymer. This system does not reveal any memory effect, as initial CNT structure was stabilized by the photo-polymerization of the polymer. EHD flows in MLC6608 + CNT system occurs in the form of turbulent flows without Kapustin–Williams domains at 20–40 V [146]. Chen et al. has also observed Kapustin–William domain pattern and some different from Kapustin–William domains in OCB cell [243].

The role of EHD instabilities is also checked by using magnetic field. Under the action of magnetic field of $H = 5$ KGs the reorientation of the planar state is noticed. Also in the case of 5CB dispersed with CNT concentration of $c = 0.01$–0.05 wt%, no memory mechanism is observed, due to the lack of EHD instabilities [41]. It was observed that MBBA/EBBA + CNT suspension shows a different dependence of σ on applied field [168]. It goes through minima at $\sim$8–11 V and then starts increasing. It is concluded that formation of fluctuating domains inside the molecular orientation generates the EHD in nematic matrix, therefore, conductivity decreases. Further the voltage at which the electrical conductivity begins to decrease becomes higher with high CNT concentration. The optical micrograph of MBBA/EBBA and MBBA/EBBA + CNT presents the appearance of EHD at 10 V and 30 V, respectively, indicating toward the suppression of onset of EHD in NLC. The change in optical texture for EBBA/MWCNTs under DC electric field is shown in Fig. 23.

Recently an interesting phenomenon of elongation of CNTs driven by electric field has been reported [39]. Up to 110 V, no appreciable stretching is observed. Above this threshold voltage, notable stretching starts and reaches to 400% in linear region, along the field direction at 170 V. Accordingly the aggregates become narrower. In this linear region, the measured length/breath strain was -6.26. The piezoelectric constant (strain/field) was 70 $(\mathrm{V}/\mu\mathrm{m})^{-1}$ along the field direction. The composites return to its original shape after field is turned off, which is associated with the higher elastic modulus of the CNT clusters. The threshold voltage required for the elongation depends on the aggregates size. The same phenomenon is also observed in isotropic phase which indicates that phenomenon is not associated with the alignment of LC director. Still images for CNT stretching and length of MWCNT clusters against the variation of electric field is shown in Fig. 24.

Induced chirality in NLC is observed by Basu and group due to dispersion of chiral CNT, which results in electroclinic effect. The observed electroclinic coefficient e_i is much smaller than the chiral nematic LCs as compared to [173,244,245]. The possible mechanism proposed is that CNTs induces tilt in the nematic LC close to its surface together with smectic fluctuation.

A simple model is introduced by Matsuyama for twist distortion in mixture of LC/CNT (rod) [246]. The critical threshold for such composite is approximately given by

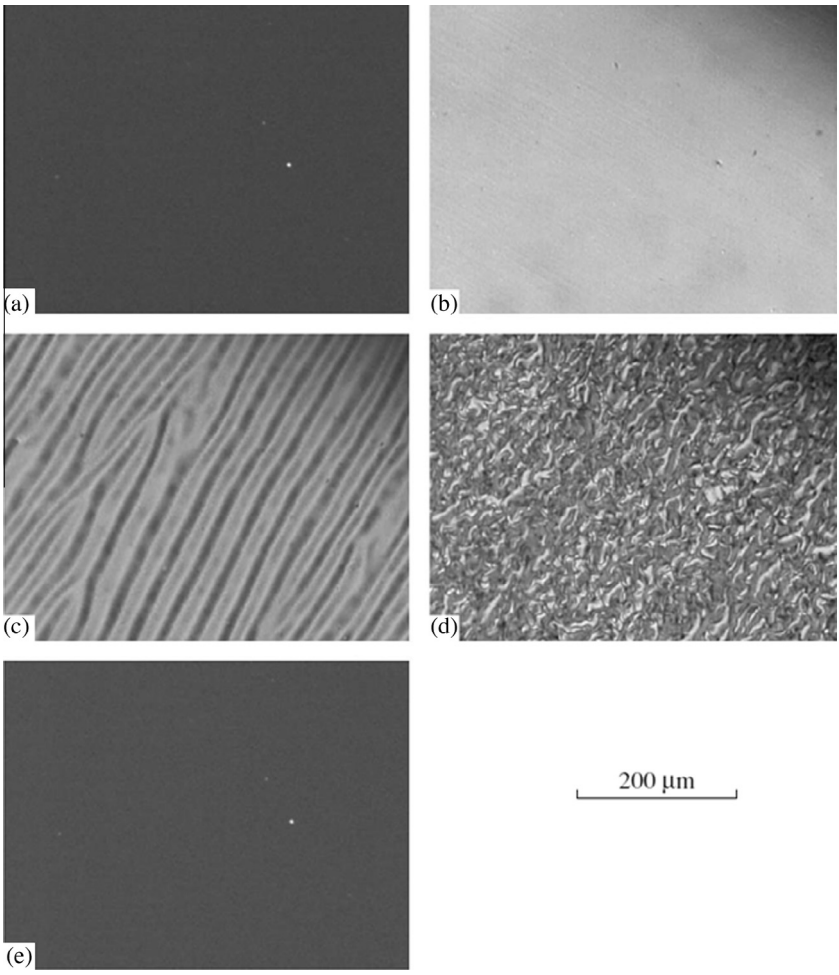

Fig. 22. Photomicrographs demonstrating changes in the structure of strongly diluted CNT suspensions in EBBA (c = 0.001 wt%) under the action of electric field (f = 2 kHz); (a) prior to the field switch on, in the field; (b) U = 10 V, t = 1 s; (c) U = 80 V, t = 5 s; (d) U = 110 V, t = 5 s and (e) after the field switch off. t is the time of action. Cells are placed in crossed polarizer so that the direction of rubbing is 450C with polarizer axes [with permission Ref. [38]].

$$H_c = \frac{\pi}{d}\sqrt{\frac{\kappa_{22,1}}{\chi_1}}\left[1+\frac{\gamma}{4}\left(\frac{d^4}{\pi^2}\right)\frac{\chi_1}{\kappa_{22,1}^2}\left(\frac{\kappa_{22,2}}{\chi_2}-1\right)\phi_2+\cdots\right] \tag{18}$$

where d is the cell gap, ϕ_2 the volume fraction of CNT, γ the coupling constant, k_{22} the twist elastic constant and χ is the magnetic anisotropy. For $\phi_2 \ll 1$, when $H > H_c$, the maximum distortion angle θ_m continuously increases with the external field H, while for $H < H_c$ the original uniform sample alignment parallel to the cell remains stable. When $\gamma = 0$ or $\phi_2 = 0$, the above equation turn out to be the critical threshold equation for pristine LC. The critical field in rod/LC composite depends on the ration $\frac{\kappa_{22,2}}{\chi_2}$ and the sign of χ_α. When $\frac{\kappa_{22,2}}{\chi_2} > 1$ the critical threshold voltage increases with rod concentration, while for $\frac{\kappa_{22,2}}{\chi_2} < 1$ the critical threshold voltage follow reverse behavior i.e. it decreases with ϕ_2. For larger magnetic or dielectric anisotropy of the rod the critical threshold decreases with increasing rod concentration and the equilibrium value of θ_m increases with ϕ_2 for $H > H_c$.

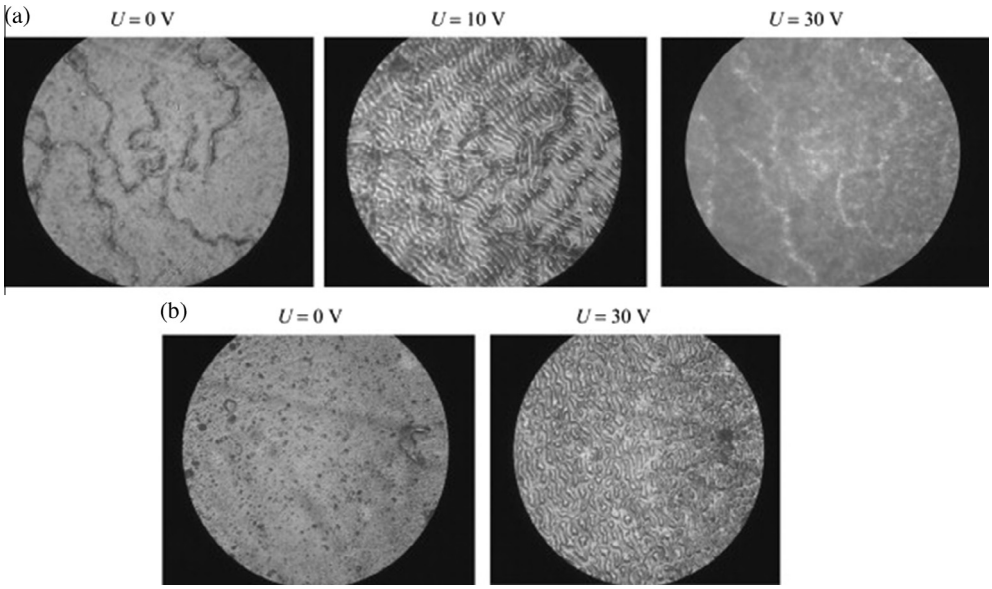

Fig. 23. Optical microscopy images of undoped (a) and doped by NT (0.02 wt%) MBBA/EBBA samples under DC electric field (image diameter corresponds to 1 mm) [with permission Ref. [168]].

10. Application of CNT/LC composite

Only very few applications of LC/CNTs have actually been realized [203,247]. An idea of magnetically steered electric switch for LC + SWCNT composite is proposed by Dierking and San [248]. It is found that for pure LC, the conductance is practically independent of the applied magnetic field, but for the LC + CNT composite the conduction increases, as CNT orients with applied magnetic field from planar to homeotropic, keeping the ac electrical voltage below the Freedericksz transition voltage. When magnetic field is turned off, the CNTs take ~4+ 0.6 s to relax back. The high sensitivity for this switch is established at low voltage and high frequency. The magnetic threshold B_{th} is found to be independent of probing voltage and frequency but inversely proportional to the cell gap d. A threshold of B_{th} = 0.4 T and B_{th} = 0.6 T for 25 μm and 15 μm cell is observed, respectively (demonstrate an electric sensor device for magnetic field).

Lai et al. [249] has proposed a sensing device based on LC + polymer + CNT composite. The proposed device has a high response time and recovery time (25 s) and also exhibited high reproducibility. Detection of acetone gas is successfully demonstrated. In another experiment gas sensor for the detection of DMMP based on CNT dispersed PDLC is demonstrated [250]. The response of the sensor is observed to be 125 s. Another application in light steered devices has also been realized recently [13]. Realization of switchable electrical insulator conductor devices such as Mott-Insulator conductor system has been reported [204]. The formation of permanent grating, under the simultaneous action of spatially modulated light and dc electric field is observed in composite [32]. Use of LC + CNT composite in electromechanical actuators is also realized [251]. A uniaxial stress of order ~1 kPa is observed in response to the field of 10^6 V/m. An idea of polarizer free guest host display is also proposed if high concentration of CNT in LC is achieved without aggregation [252]. Another perspective of application of LC/CNT composite in storage devices have been realized by Yaroshchuk and workers [196]. LC/CNT suspension has already proved its applicability in dynamic holography, image processing, four wave mixing, beam amplification, etc. owing to their extensive photo-refractive properties.

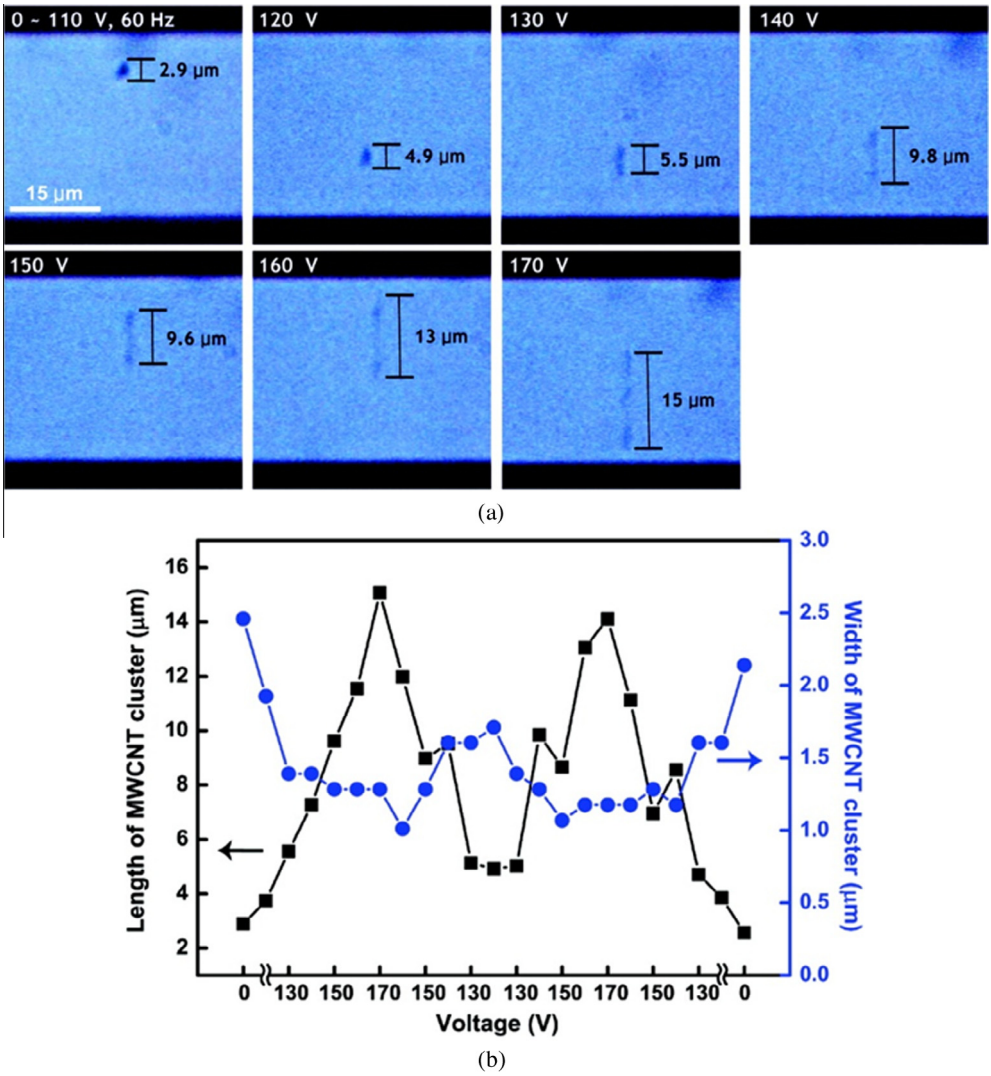

Fig. 24. (a) Still cut images of one CNT aggregate depending on the applied voltage. The measuring rod depicts the length of CNT aggregates. (b) Voltage dependent width and length of a CNT cluster [with permission Ref. [39]].

11. Conclusion and future perspectives

Liquid crystals are state of matter sharing symmetry and properties that are usually associated with both solids and liquids. Their study belongs to the wider field of soft condensed matter physics, an area growing in importance because of new physics being discovered and the possibilities of various technological applications being developed. On the other hand, Carbon nanotubes are tubular cylinders of carbon atoms that have extraordinary mechanical, electrical, thermal, optical and chemical properties. It is of great interest and current area of research to investigate the influence of dispersion of nanomaterials (nanoparticles, quantum dots, CNTs, etc.) in LCs and study now the structure and properties change so that the LC/nanomaterials systems can be tailored for the applications. LC/CNT suspension has become an area of great interest, in recent years, due to their potential

applicability in display devices, sensors, actuators, switches, etc. It has become obvious that enthralling electrical, optical and electro-optical properties of LC/CNT suspension has made it convincing for various engineering relevance. A number of research papers published in the last few years signify its importance. Much effort has been devoted for the basic understanding of physics of the suspension. In this review article, the method of aligning CNTs, dispersion of CNTs in LCs is briefly discussed and more attention has been paid on the effect of CNTs on various properties of LCs. The effect of electric/-magnetic field on NLC/CNT suspension is also explored including some interesting observations such as superelongation of nanotubes, electrohydrodynamic instabilities and four lobe textures. The potential applications of such suspension have also been discussed.

The existing strong dipole–dipole interaction among the tubes due to greater polarizability along the tube axis, leads to the requirement of strongly polar or highly polarizable liquid crystal to effectively disperse the nanotubes. Some liquid crystals such as 5CB and E7 follow the same criteria. The high dipole moment of LC molecules will lead to the increased interaction between CNT and LC molecules. At the same time, the strong interaction between LC molecules will lead to an antiparallel orientation. This will lower down the possibility of dispersing CNT effectively. Therefore, LC with medium dipole moment is preferred for the dispersion of CNTs. Orientation of the CNTs can be achieved by imposing the self organizing capability of the LC molecules to CNTs. The inherent orientational order of LCs can be easily switched to CNTs. The free energy of the LC/CNT suspension is minimum when CNTs are aligned along the director. Also, the strong interaction between nanotubes and LC molecules, in the form of π–π stacking consequences well structured nanotubes inside the nematic matrix. The low concentration of CNTs in LCs is found to be well dispersed and oriented, however, higher lending lead to the aggregation. At higher loading of CNTs in LCs, the Vander Waals forces become strong enough to cause the aggregation.

The structural resemblance of CNTs and LCs escorts the LCs to integrate CNTs into its own configuration effortlessly and also nanotubes efficiently enhance the electrical, optical and electro-optical properties of LCs. It is experimentally established that even a very minute concentration of nanotubes in LC have very reflective effect on the LC mechanism. It has been realized that minute concentration of CNTs in LCs works as an inert filler and does not appreciable change the nematic to isotropic transition. However, higher loading ($c \sim 0.1$ wt%) leads to a significant enhancement of the T_{NI} temperature. It is worth mentioning here that transition from I–N and N–SmA remains first order and second order, respectively. Recent results show that CNTs effectively reduces the ion density and suppress the screening effect. This results in reduced threshold voltage and simultaneously reduces the rotational viscosity. A comparative study of C–V and T–V curve reveals that hysteresis width decreases with the dispersion of CNT in LC. There exist an optimal concentration of nanotubes in LC, where improvement to display parameters such as threshold voltage, response time, low hysteresis is observed. It should be kept in mind that improvement of the LC properties depends upon the interaction of LC and tubes which further depends upon the LC material and dispersion quality of the nanotubes. LC/CNT suspension has shown its potential to the application in dynamic holography, image processing, four wave mixing and optical computing other than sensors, display and actuators. Another perspective of application of LC/CNT composite in storage devices has also been realized. An irreversible electro-optical effect pilots to the observed memory effect in suspension. The sustained planar state, even when the field if turned off is responsible for the residual transmittance. One should also remember here that effect of the CNTs on liquid crystal properties can be distinct, depending on the extent of the interaction between CNTs and LC molecules. The interaction further depends on chemical nature of LC and CNT, the aspect ratio of CNT and the purity of both the samples.

Even though well aligned CNTs at some low concentration in LC is achieved, yet at some high concentration, generally $c > 0.1$ wt% the formation of aggregates is of prime concern. Also, it is realized that low concentration of CNTs in LC are not stable and get sediment with the passage of time. This shrinks the applicability area of the suspension. Much effort is still needed to achieve aligned CNTs in LC at large scale. There are few reports over dispersion of nanotubes inside lyotropic liquid crystal and very few over dispersion in smectic phases. The research of this area is at infancy level. The field of CNT dispersion in blue phases and some highly ordered smectic phases is untouched. Also the investigation of other applicability of LC/CNT suspension is yet to be done. Therefore, a combined effort from physics, chemistry and engineering is needed to fully see the sights of this field. There is no doubt

an imperative part of LC/CNT suspension is yet to come. In upcoming years we will be acquainted with more fundamental knowledge about the suspension including physics, chemistry and engineering. Therefore, future of LC/CNT suspension seems to be very promising and more application is yet to be discovered.

Acknowledgements

Authors are grateful to Department of Science and Technology (DST) New Delhi, India for financial support. The authors also thank corresponding publishers/authors for their kind permission to reproduce their figures.

References

[1] Saito R, Dresselhaus G, Dresselhaus MS. Physical properties of carbon nanotubes. London, UK: Imperial College press; 1998.
[2] Harris PJF. Carbon nanotubes and related structures. Cambridge, UK: Cambridge University Press; 1999.
[3] Ajayan PM. Chem Rev 1999;99:1787–99.
[4] Sinott SB, Andrews R. Crit Rev Solid State Mater Sci 2001;26:145–249.
[5] Banghman RH, Zakhidov AA, de Heer WA. Science 2002;297:787–92.
[6] Ch Postma HW, Teepen T, Yao Z, Grifoni M, Dekker C. Science 2001;293:76–9.
[7] Dalton AB, Collins S, Muñoz E, Razal JM, Ebron VH, Ferraris JP, et al. Nature 2003;423:703.
[8] Tseng YC, Xuan P, Javey A, Malloy R, Wang Q, Bokor J, et al. Nano Lett 2004;4:123–7.
[9] Zhang M, Fang S, Zakhidov AA, Lee SB, Aliev AE, Williams CD, et al. Science 2005;309:1215–9.
[10] Vairavapandian D, Vichchulada P, Lay MD. Anal Chim Acta 2008;626:119–29.
[11] Arico AS, Bruce P, Scrosati B, Tarascon JM, Schalkwijk W. Nat Mater 2005;4:366–77.
[12] Lynch MD, Patrick DL. Nano Lett 2002;2:1197–201.
[13] Dierking I, Scalia G, Morales P, LeClere D. Adv Mater 2004;16:865–9.
[14] Schoot PD, Popa-Nita V, Kralj S. J Phys Chem B 2008;112:4512–8.
[15] Weiss V, Thiruvengadathan R, Regev O. Langmuir 2006;22:854–6.
[16] Kumar S, Bisoyi HK. Angew Chem Int Ed 2007;46:1501–3.
[17] Lagerwall J, Scalia G, Haluska M, Weglikowska UD, Roth S, Giesselmann F. Adv Mater 2007;19:359–64.
[18] Heilmeier GH, Zanoni LA. Appl Phys Lett 1968;31:91–2.
[19] Pozhidaev EP, Ganzke D, Zyryanov VYa, Smorgon SL, Haase W. Liq Cryst 2002;29:1305–10.
[20] Manohar R, Misra AK, Srivastava AK. Polym Compos 2010;31:1776–81.
[21] Prasad SK, Sandhya KL, Nair GG, Hiremath US, Yelamaggad CV, Sampath S. Liq Cryst 2006;33:1121–5.
[22] Manohar R, Yadav SP, Srivastava AK, Misra AK, Pandey KK, Sharma PK, et al. Jpn J Appl Phys 2009;48(101501):1–6.
[23] Ouskova E, Buchnev O, Reshetnyak V, Reznikov Y, Kresse H. Liq Cryst 2003;30:1235–9.
[24] Reznikov Y, Buchnev O, Tereshchenko O, Reshetnyak V, Glushchenko A, West J. Appl Phys Lett 2003;82:1917–9.
[25] Lee WK, Hwang SJ, Cho MJ, Park HG, Han JW, Song S, et al. Nano Scale 2013;5:193–9.
[26] Tong X, Zhao Y. J Am Chem Soc 2007;129:6372–3.
[27] Dierking I, Scalia G, Morales P. J Appl Phys 2005;97:044309-1–9-5.
[28] Roussel F, Brun JF, Allart A, Huang L, Brien SO. AIP Adv 2008;2:012110-1–0-9.
[29] Manohar R, Pandey KK, Srivastava AK, Misra AK, Yadav SP. J Phys Chem Solids 2010;71:1311–5.
[30] Yadav SP, Pandey KK, Misra AK, Tripathi PK, Manohar R. Phys Scr 2011;83:035704-1–4-5.
[31] Yadav SP, Pande M, Manohar R, Singh S. Liq Cryst 2013;40:1503–11.
[32] Lee W, Chen HC. J Phys D Appl Phys 2002;35:2260–3.
[33] Lee W, Chen HY, Yeh SL. Opt Express 2002;10:482–7.
[34] Ion FM, Berezovski C, Berezovski R, Heimann G, Moisescu M. Romanian Rep Phys 2012;64:1011–8.
[35] Chen HY, Lee W. Opt Rev 2005;12:223–5.
[36] Kovalchuk A, Dolgov L, Yaroshchuk O. Semiconduct Phys Quant Electron Optoelectron 2008;11:337–41.
[37] Lisetski LN, Minenko SS, Ponevchinsky VV, Soskin MS, Goncharuk AI, Lebovka NI. Mat-wiss U Werstofftech 2011;42:5–14.
[38] Dolgov LA, Lebovka NI, Yaroschuk OV. Colloid J 2009;71:603–11.
[39] Jeong SJ, Park KA, Jeong SH, Jeong HJ, An KH, Nah CW, et al. Nano Lett 2007;7:2178–82.
[40] Dolgov LA, Yaroshchuk O, Tomylko S, Lebovka N. Condens Matter Phys 2012;15:33401–1–8.
[41] San SE, Okutan M, Koysal O, Yerli Y. Chin Phys Lett 2008;25:212–5.
[42] Basu R, Iannacchione GS. Appl Phys Lett 2008;93:183105-1–5-3.
[43] Lu SY, Chien LC. Opt Express 2008;16:12777–85.
[44] Lee W, Wang CY, Shih YC. Appl Phys Lett 2004;85:513–5.
[45] Lee W, Gau JS, Chen HY. Appl Phys B 2005;81:171–5.
[46] Rahman M, Lee W. J Phys D Appl Phys 2009;42:063001-1–063001-12.
[47] Lagrwall JPF, Scalia G. J Mater Chem 2008;18:2890–8.
[48] Zakri C. Liq Cryst Today 2007;16:1–11.
[49] Schymura S, Scalia G. Philos Trans Roy Soc A 2013;371:2012061-1–2012061-14.
[50] Stamatoin D, Mirzaei J, Feng X, Hegmann T. Top Curr Chem 2012;318:331–94.
[51] Blanc C, Coursault D, Lacase E. Liq Cryst 2013;1:83–109.
[52] de Gennes PG, Prost J. The physics of liquid crystals. New York, USA: Oxford University Press; 1995.

[53] Chandrsekhar S. Liquid crystals. Cambridge, UK: Cambridge University Press; 1992.
[54] Singh Shri, Dunmur DA. Liquid crystals: fundamentals. Singapore: World Scientific Publishing; 2002.
[55] Oswald P, Pieranski P. Nematic and cholesteric liquid crystals: concept and physical properties illustrated by experiments. USA: CRC Press; 2005.
[56] Li Q. Liquid crystals beyond display: chemistry, physics and applications. New Jersey, Canada: John Wiley & Sons; 2012.
[57] Blinov LM, Chigrinov VG. Electrooptic effects in liquid crystal materials. New York: Springer-Veralg; 1996.
[58] Blinov LM. Electrooptic and magnetooptic properties of liquid crystals. New Jersey: John Wiley & Sons; 1983.
[59] Tans SJ, Devoret MH, Dai H, Thess A, Smalley RE, Geerlings LJ, et al. Nature 1997;386:474–7.
[60] Tasis D, Tagmatarchis N, Bianco A, Prato M. Chem Rev 2006;106:1105–36.
[61] Park TJ, Banerjee S, Benny TH, Wong SS. J Mater Chem 2006;16:141–54.
[62] Bahr JL, Tour JM. J Mater Chem 2002;12:1952–8.
[63] Xie XL, Mai YW, Zhou XP. Mater Sci Eng R 2005;49:89–112.
[64] Iijima S. Nature 1991;354:56–8.
[65] Iijima S, Ichihashi T. Nature 1993;363:603–5.
[66] Colbert DT et al. Science 1994;266:1218–22.
[67] Liu J et al. Science 1998;280:1253–6.
[68] Wong EW, Sheehan PE, Lieber CM. Science 1997;277:1971–5.
[69] Thonstenson ET, Ren Z, Chou TW. Compos Sci Technol 2001;61:1899–912.
[70] Ebbesen TW, Ajayan PM. Nature 1992;358:220–2.
[71] Thess A et al. Science 1993;273:483–7.
[72] Yacaman MJ, Yoshida MM, Rendon L, Santiesteban JG. Appl Phys Lett 1993;62:657–9.
[73] Lie WZ, Xie SS, Qian LX, Chang BH, Zoa BS, Zhou WY, et al. Science 1996;274:1701–3.
[74] Ren ZF, Huang ZP, Xu JW, Wang JH, Bush P, Siegal MP, et al. Science 1998;282:1105–7.
[75] Hata K, Futaba DN, Mizuno K, Namai T, Yumura M, Iijima S. Science 2004;306:1362–4.
[76] Nikolaev P, Bronikowski MJ, Bradley RK, Rohmund F, Colbert DT, Smith KA, et al. Chem Phys Lett 1999;313:91–7.
[77] Rafique MMA, Iqbal J. J Encapsul Adsorpt Sci 2011;1:29–34.
[78] Tanaka T et al. Nano Lett 2009;9:1497–500.
[79] Tanaka T, Urabe Y, Nishide D, Kataura H. Appl Phys Express 2009;2:125002-1–2-3.
[80] Belluci S. Phys Stat Sol (C) 2005;2:34–47.
[81] Demczyk BG, Wang YM, Cumings J, Hetman M, Han W, Zettl A, et al. Mater Sci Eng A 2002;334:173–8.
[82] Palaci I, Fedrigo S, Brune H, Klinke C, Chen M, Riedo E. Phys Rev Lett 2005;94:175502-1–2-4.
[83] Meo M, Rossi M. Compos Sci Technol 2006;66:1597–605.
[84] Hong S, Myung S. Nat Nanotechnol 2007;2:207–8.
[85] Takesue I, Haruyama J, Kobayashi N, Chiashi S, Maruyama S, Sugai T, et al. Phys Rev Lett 2006;96:057001-1–1-4.
[86] Sinha S, Barjami S, Iannacchione G, Schwab A, Muench G. J Nanopart Res 2005;7:651–7.
[87] Pop E, Mann D, Wang Q, Goodson K, Dai H. Nano Lett 2005;6:96–100.
[88] Thostenson E, Li C, Chou T. Compos Sci Technol 2005;65:491–516.
[89] Sun X, Chen T, Yang Z, Peng H. Angew Chem Int Ed 2013;46:539–49.
[90] Piao G, Kimura F, Takahashi T, Moritani Y, Awano H, Nimori S, et al. Pol J 2007;39:589–92.
[91] Jang BK, Sakka Y, Woo SK. J Phys: Conf Ser 2009;156:012005.
[92] Xie XL, Mai YW, Zhou XP. Mater Sci Eng R: Rep 2005;49:89–112.
[93] Orofeo CM, Ago H, Yoshihara N, Tsuji M. J Novel Carbon Resour Sci 2010;2:36–40.
[94] Zhao H, Zhou Z, Dong H, Zhang L, Chen H, Hou L. Sci Rep 2013;3:1–5 3480.
[95] Mahanandaia P, Nanda KK. Nanotechnology 2008;19:155602-1–2-7.
[96] Ren Z, Lan Y, Vang Y. Aligned carbon nanotubes: physics concept, fabrication and devices. Heidelberg, New York, London: Springer; 2013.
[97] Braford PD, Wang X, Zhao H, Maria JP, Jia Q, Zhu YT. Compos Sci Technol 2010;70:1980–5.
[98] Orofeo CM, Ago H, Yoshihara N, Tsuji M. Appl Phys Lett 2009;94:053113.
[99] Iakoubovskii K. Cent Eur J Phys 2009;7:645–53.
[100] Kumar Mukul. Carbon nanotube synthesis and growth mechanism, carbon nanotubes - synthesis, characterization, applications. In: Yellampalli Siva, editor. InTech; 2011. http://dx.doi.org/10.5772/19331. ISBN: 978-953-307-497-9.
[101] Meyyappan M, Delzeit L, Cassell A, Hash D. Plasma Sources Sci Technol 2003;12:205–16.
[102] Sen S, Puri IK. Nanotechnology 2004;15:264–8.
[103] Pumera M. Langmuir 2007;23:6453–8.
[104] Edwards ER, Antunes EF, Botelho EC, Baldon MR, Corat EJ. Appl Surf Sci 2011;258:641–8.
[105] Ago H et al. J Nanosci Nanotechnol 2008;8:6165.
[106] Chen W, Tao X. Appl Surf Sci 2006;252:3547.
[107] Dai L, Patil A, Gong X, Guo Z, Liu L, Liu Y, et al. Chem Phys Chem 2003;4:1150–69.
[108] Qin LC, Zhao X, Hirahara K, Miyamoto Y, Ando Y, Iijima S. Nature 2000;408:50.
[109] Suh JS, Lee JS. Appl Phys Lett 1999;75:2047–50.
[110] Sinha AK, Hwang DW, Hwang LP. Chem Phys Lett 2000;332:455–60.
[111] Jin L, Bower C, Zhou O. Appl Phys Lett 1997;73:1197–999.
[112] Bendiab N, Almairac R, Sauvajot JL, Rols S, Elakim E. J Appl Phys 2003;93:1769–73.
[113] Lanticse LJ, Tanabe Y, Matsui K, Kaburagi Y, Suda K, Hoteida M, et al. Carbon 2006;44:3078. 3078-.
[114] Watts PCP, Lynth SM, Meudoza E, Ravi S, Silva P. Appl Phys Lett 2006;89:103113-1–3-3.
[115] de Heer WA et al. Science 1995;268:845–7.
[116] Nicholas A et al. ACS Nano 2010;4:3969–78.
[117] Yonemura H, Yamamoto Y, Yamda S, Fujiwara Y, Tanimoto Y. Sci Technol Adv Mater 2008;9:024213-1–3-6.
[118] Zhou Z, Wan D, Dou X, Song L, Zhou W, Xie S. Carbon 2006;44:170–3.
[119] Xin H, Woolley AT. Nano Lett 2004;4:1481–4.

[120] Kim Y, Minami N, Zhu W, Kazaoui S, Azumi R, Matsumoto M. Jpn J Appl Phys 2003;42:7629–34.
[121] Nuriel S, Liu L, Barber AH, Wagner HD. Chem Phys Lett 2005;404:263–6.
[122] Hilding J, Grulke EA, Zhang ZG, Lockwood F. J Disper Sci Technol 2003;24:1–41.
[123] Furtado CA, Kim UJ, Gutierrez HR, Pan L, Dickey EC, Eklund PC. J Am Chem Soc 2004;126:6095–105.
[124] Hasan T, Scardaci V, Tan PH, Rozhin AG, Milne WI, Ferrari AC. J Phys Chem C 2007;111:12594–602.
[125] Dumonteil S, Demortier A, Detriche S, Raes C, Fonseca A, Rühle M, et al. J Nanosci Nanotechnol 2006;6:1315–8.
[126] Cheng Q. Dispersion of single-walled carbon nanotubes in organic solvents. Doctoral thesis. Dublin: Dublin Institute of Technology; 2010.
[127] Maeda Y et al. J Phys Chem B 2004;108:18395–7.
[128] Islam MF, Rojas E, Bergey DM, Johnson AT, Yodh A. Nano Lett 2003;3:269–73.
[129] Wenseleers W, Vlasov II, Goovaerts E, Obraztsova ED, Lobach AS, Bouwen A. Adv Funct Mater 2004;14:1105–12.
[130] Nakashima N, Okuzeno S, Murakami H, Nakai T, Yoshikawa K. Chem Lett 2003;32:456–7.
[131] Badaire S, Zakri C, Maugey M, Derre A, Barisci JN, Wallace GG, et al. Adv Mater 2005;17:1673–6.
[132] Moulton SE, Maugey M, Poulin P, Wallace GG. J Am Chem Soc 2007;129:9452–7.
[133] Chen J, Hamon MA, Hu H, Chen Y, Rao AM, Eklund PC, et al. Science 1998;282:95–8.
[134] Hamon MA, Chen J, Hu H, Chen Y, Itkis ME, Rao AM, et al. Adv Mater 1999;11:834–40.
[135] Karajanagi SS, Yang HC, Asuri P, Sellitto E, Dordick JS, Kane RS. Langmuir 2006;22:1392–5.
[136] Chen J et al. J Phys Chem B 2001;105:2525–8.
[137] Chen HY, Lee W, Clark NA. Appl Phys Lett 2007;90:033510-1–0-3.
[138] Basu R, Chen CL, Rosenblatt C. J Appl Phys 2011;109:083518-1–8-4.
[139] Ji Y, Huang YY, Terentjev EM. Langmuir 2011;27:13254–60.
[140] Trushkevych O, Collings N, Hasan T, Scardaci V, Ferrari AC, Wilkinson TD, et al. J Phys D Appl Phys 2008;41(125106):1–11.
[141] Chen X, Wu X, Zou J, Liu J, Chen J. Mater Sci Eng B 2011;176:425–30.
[142] Lesetski LN, Chepikov AM, Minenko SS, Lebovka NI, Soskin MS. Funct Mater 2011;18:143–8.
[143] Schymura S, Kuhnast M, Lutz V, Jagiella S, Wenglikowska UD, Roth S, et al. Adv Funct Mater 2010;20:3350–7.
[144] Yoo HJ, Lee SY, You NH, Lee DS, Yeo H, Choi YM, et al. Synth Met 2013;181:10–7.
[145] Tie W, Yang GH, Bhattacharyya SS, Lee YH, Lee SH. J Phys Chem C 2011;115:21652–8.
[146] Dolgov L, Yaroshchuk O, Lebovka M. Mol Cryst Liq Cryst 2008;496:212–29.
[147] Song W, Windle AH. Macromolecules 2005;38:6181–8.
[148] Yaroshchuk O, Tomylko S, Kovalchuk O, Lebovka N. Carbon 2014;68:389–98.
[149] Lebovka N, Dadakova T, Lysetskiy L, Melezhyk O, Puchkovska G, Gavrilko T, et al. J Mol Struct 2008;887:135–43.
[150] Scalia G, Lagerwall JPF, Haluska M, Weglikowska UD, Giesselmann F, Roth S. Phys Stat Sol B 2006;243:3238–41.
[151] Jber NR, Rashad AA, Shihab MS. J Mol Struct 2013;1043:28–36.
[152] Park KA, Lee SM, Lee SH, Lee YH. J Phys Chem C 2007;111:1620–4.
[153] Jeong SY, Park KH, Baik I, Jeong SJ, Jeong SH, An KH, et al. NANO 2007;2:41–9.
[154] Baik IS, Jeon SY, Jeong SJ, Lee SH, An KH, Jeong SH, et al. J Appl Phys 2006;100(15):074306.
[155] Brochard F, de Gennes PG. J Phys 1970;31:691–708.
[156] Burylov SV, Raikher YL. Phys Lett A 1990;149:279–83.
[157] Burylov SV, Raikher YL. Phys Rev E 1994;50:358–67.
[158] Andrienko D, Allen MP. Phys Rev E 2002;65:041702-1–2-7.
[159] Andrienko D, Tasinkevych M, Patricio P, Allen MP, Telo da Gama MM. Phys Rev E 2003;68:051702-1–2-5.
[160] Hung FR, Guzmán O, Gettelfinger BT, Abbott NL, de Pablo JJ. Phys Rev E 2006;74:011711-1–011711-12.
[161] Krasna M, Cvetlko M, Ambrozic M. Beilstein J Org Chem 2010;6:74.
[162] Scalia G, Lagerwall JPF, Schymura S, Haluska M, Giesselmann F, Roth S. Phys Stat Sol B 2007;244:4212–7.
[163] Zhao W, Wang J, He J, Zhang L, Wang X, Li R. Appl Surf Sci 2009;255:6589–92.
[164] Adams PM, Mallon JJ. Mol Cryst Liq Cryst 1991;208:65–75.
[165] Juhl AT, Yang DK, Tondiglia VP, Natarajan LV, White TJ, Bunning TJ. Opt Mater Express 2011;1:1536–47.
[166] Kamanina NV, Vasilyev PY, Studeonov VI. Theoret Appl Mech 2011;38:37–46.
[167] Russell JM, Oh S, Larue I, Zhou O, Samulski ET. Thin Solid Films 2006;509:53–7.
[168] Lisetski LN, Minenko SS, Fedoryako AP, Lebovka NI. Physica E 2009;41:431–5.
[169] Puech N, Dennison M, Blanc C, Schoot PV, Dijkstra M, Roij RV, et al. Phys Rev Lett 2012;108:247801-1–1-5.
[170] Goncharuk AI, Lebovka NI, Lisetski LN, Minenko SS. J Phys D Appl Phys 2009;42(165411):1–8.
[171] Ponevchinsky VV, Vasilev VI, Soskin MS, Goncharuk AI, Lebovka NI. arxiv:0911.0808V1 [cond-mat.mes-hall]; 2009.
[172] Kaya N, Akkurt F, Alicilar A. Fullerenes Nanotubes Carbon Nanostruct 2011;19:262–70.
[173] Akkurt F. Liq Cryst 2014;41:1269–76.
[174] Minenko SS, Lisetski LN, Goncharuk AI, Lebovka NI, Ponevchinsky VV, Soskin MS. Funct Mater 2010;17:454–9.
[175] Petrov M, Katranchev B, Rafailov PM, Naradikian H, Dettlaf-Weglikowska U, Keskinova E, et al. J Phys: Conf Ser 2012;398:012035-1–5-6.
[176] Lagerwall JPF, Scalia G, Haluska M, Dettlaf-Weglikowska U, Giesselmann F, Roth S. Phys Stat Sol B 2006;243:3046–9.
[177] Buluy O, Nepijko S, Reshetnyak V, Ouskova E, Zadorozhnii V, Leonhardt A, et al. Soft Matter 2011;7:644–9.
[178] Popa-Nita V, Kralj S. J Chem Phys 2010;132:024902-1–2-8.
[179] Kralj S, Bradac Z, Popa-Nita V. J Phys: Condens Matter 2008;20:244112-1–2-7.
[180] Nita VP, Cevko M, Kralj S. Liquid crystal anisotropic nanoparticles mixture. In: Marulanda JM, editor. Electronic properties of carbon nanotubes. Intechopen; 2011 [chapter 29].
[181] Duran H, Gazdecki B, Yamashita A, Kyu T. Liq Cryst 2005;32:815–21.
[182] Jo EM, Srivastava AK, Bae JJ, Kim M, Lee MH, Lee HK, et al. Mol Cryst Liq Cryst 2009;498:74–82.
[183] Sigdel KP, Iannacchione GS. Eur Phys J E 2011;34:34–42.
[184] Shah HJ, Fontecchio AD, Mattia D, Gogotsi Y. J Appl Phys 2008;103:064314-1–4-5.
[185] Lebovka N, Melnyk V, Mamumya Y, Klishevich G, Goncharuk A, Pivovarova N. Physica E 2013;52:65–9.
[186] Mitroova Z et al. New J Chem 2011;35:1260–4.

[187] Mitróová Z et al. Phys Procedia 2010;9:41–4.
[188] Mitroova Z et al. Magnetohydrodynamics 2009;45:353–60.
[189] Hosaka S, Tozaki K, Hayashi H, Inaba H. Physica B 2003;337:138–46.
[190] Petrov M, Katranchev B, Rafailov PM, Naradikian H, Dettlaf-Weglikowska U, Keskinova E, et al. Phys Rev E 2013;88:042503.
[191] Popa-Nita V, Bucek S. Phys Res Int 2012. http://dx.doi.org/10.1155/2012/750890.
[192] Lisetski LN, Lebovka NI, Sidletskiy OT, Panikarskaya VD, Kasian NA, Kositsyn SS, et al. Funct Mater 2007;14:233–7.
[193] Lysetskiy L, Panikarskaya V, Sidletskiy O, Kasian N, Kositsym S, Shtifanyuk P, et al. Mol Cryst Liq Cyrst 2007;478:883–9.
[194] Basu R, Innacchione GS. J Appl Phys 2009;106:124312-1–2-6.
[195] Basu R, Iannacchione GS. Appl Phys Lett 2009;95:173113-1–3-3.
[196] Yaroshchuk O, Tomylko S, Dolgov L, Semikina T, Kovalchuk O. Diam Relat Mater 2010;19:567–72.
[197] Glushchenko A, Yaroshchuk O. Mol Cryst Liq Cryst 1999;330:415–22.
[198] Glushchenko A, Kresse H, Reshetnyak V, Reznikov Yu, Yaroshchuk O. Liq Cryst 1997;23:241–6.
[199] Lee CW, Shih WP. Mater Lett 2010;64:466–8.
[200] Baik IS, Jeon SY, Lee SH, Park KA, Jeong SH, An KH, et al. Appl Phys Lett 2005;87:263110-1–0-3.
[201] Huang CY, Pan HC. Appl Phys Lett 2006;89:056101-1–1-2.
[202] Jeon SY, Lee SH, Lee YH. Appl Phys Lett 2006;89:056102-1.
[203] Kumar MV, Prasad SK. Nano Syst: Phys Chem Math 2013;4:425–9.
[204] Khushboo, Malik P, Chaudhary A. J Adv Phys 2014;4:565–70.
[205] Rahman M, Lee W. Key Eng Mater 2010;428–429:173–81.
[206] Trushkevych F, Goldeen M, Pivnenko H, Xu N, Coolings WA, Crossland S, et al. Electron Lett 2010;46:693–5.
[207] Nayek P, Roy S, Dabrowski R. J Nanosci Nanotechnol 2012;12:6216–23.
[208] Garcia AG, Vergaz R, Algorri JF, Quintana X, Oton JM. Beilstein J Nanotechnol 2015;6:396–403.
[209] Jian BR, Tang CY, Lee W. Carbon 2011;49:910–4.
[210] Jayalakshmi V, Prasad SK. Appl Phys Lett 2009;94(202106):1–3.
[211] Shah HJ, Pontecchio AK, Mattia D, Gogotsi Y. J Appl Phys 2008;103:064314-1–4-5.
[212] Cirtoaje C, Petrescu E, Motoc C. Physica E 2013;54:242–6.
[213] Nayek P, Ghosh S, Karan S, Kang SW, Roy SK, Dabrowski R. Jpn J Appl Phys 2011;50(121701):1–6.
[214] Basu R, Iannacchione GS. Phys Rev E 2010;81:051705-1–5-5.
[215] Prasad SK, Kumar MV, Yelamaggad CV. Carbon 2013;59:512–7.
[216] Fuh AYG, Lee W, Huang KYC. Liq Cryst 2013;40:745–55.
[217] Sihova A. Prog Electromagn Res 2005;51:65–82.
[218] Basu R. Appl Phys Lett 2013;103:241906.
[219] Huang CY, Hu CY, Pan HC, Lao KY. Jpn J Appl Phys 2005;44:8077.
[220] Huang CY, Lin YG, Huang YT. Jpn J Appl Phys 2008;47:6407.
[221] Abbasov ME, Carlisle GO. J Mater Sci: Mater Electron 2012;23:712–7.
[222] Jeon SY, Shin SH, Jeong SJ, Lee SH, Jeong SH, Lee YH, et al. Appl Phys Lett 2007;90:121901-1–1-3.
[223] Dierking I, Casson K, Hampson R. Jpn J Appl Phys 2008;47:6390–3.
[224] Georgiev GY, Gombas EA, Melutype MB, Mattera MP, Gati PA, Cabrera Y, et al. MRS proceeding, 1228, 1228-kk11-81; 2009.
[225] Lee HK, Lee SE, Kang BG, Jeon EJ, Lim YJ, Lee K, et al. Mol Cryst Liq Cryst 2010;530:157–62.
[226] Hsu JS, Chang WJ, Hu CY, Li HC. Jpn J Appl Phys 2009;48:020220-1–0-2.
[227] Lee W, Chen HY. Jpn J Appl Phys 2007;46:2962–7.
[228] Lin FC, Wu PC, Jian BR, Lee W. Adv Condens Matter Phys 2013. http://dx.doi.org/10.1155/2013/271574.
[229] Liu HH, Lee W. Appl Phys Lett 2010;97:173501-1–1-3.
[230] Jeon SY, Shin SH, Lee JH, Lee SH, Lee YH. Jpn J Appl Phys 2007;46:7801–2.
[231] Chen HY, Lee W. Appl Phys Lett 2006;88:222105-1–5-3.
[232] Lee W, Yeh SL. Appl Phys Lett 2001;79:4488–90.
[233] Lee W, Yeh SL, Chang CC, Lee CC. Opt Express 2001;9:791–5.
[234] Lee W, Hsiao KC. Appl Phys B: Laser Opt 2004;78:377–80.
[235] Lee W, Hsiao KC. Appl Phys B: Laser Opt 2004;78:351–4.
[236] Ghosh S, Carlisle GO. J Mater Sci: Mater Electron 2005;16:753–9.
[237] Abbagov ME, Carlisle GO. J Nanophoton 2008;2:023510.
[238] Khoo IC, Ding J, Zhang Y, Chen K, Diaz A. Appl Phys Lett 2003;82:3587–9.
[239] Khoo IC, Zang Y, Diaz A, Ding J, Chen K. Proc SPIE 5213, Liquid Crystal VII, 2003:139.
[240] Chen YN, Wu JJ, Le HL. Jpn J Appl Phys 2008;47:8631–4.
[241] Jeong SJ, Sureshkumar P, Jeong KU, Srivastava AK, Lee SH, Jeong SH, et al. Opt Express 2007;15:11698–705.
[242] Srivastava AK, Jeong SJ, Lee MH, Lee SH, Jeong SH, Lee YH. J Appl Phys 2007;102:043503-1–3-5.
[243] Chen YN, Wu JJ, Ke HL. Jpn J Appl Phys 2008;47:8487–90.
[244] Basu R, Petschek RG, Rosenblatt C. Phys Rev E 2011;83:041707-1–7-4.
[245] Basu R, Rosenblatt C, Lemieux RP. Liq Cryst 2012;39:199–204.
[246] Matsuyama A. Liq Cryst 2011;38:885–91.
[247] Qi H, Hegmann T. J Mater Chem 2008;18:3288–94.
[248] Dierking I, San SE. Appl Phys Lett 2005;87:233507-1–7-3.
[249] Lai YT, Kuo JC, Yang YJ. Sensors Actuat A 2014;215:83–8.
[250] Lai YT, Kuo JC, Yang YJ. Appl Phys Lett 2013;102:191912-1–2-3.
[251] Courty S, Mine J, Tajbakhsh AR, Terentjev EM. Europhys Lett 2003;64:654–60.
[252] Scalia G, Buhler CV, Hagele C, Roth S, Giesselmann F, Lagerwall JPF. Soft Matter 2008;4:570–6.